AD-A047 489 STATE UNIV OF NEW YORK AT BUFFALO FACULTY OF ENGINEER--ETC F/G 20/11
LASER INDUCED THERMOELASTIC RESPONSE OF CIRCULAR PLATES.(U)
OCT 77 H REISMANN, D MALONE, P S PAWLIK AFOSR-76-2943

UNCLASSIFIED AFOSR-TR-77-1286 NL

1 OF 1
AD
A047489

END
DATE FILMED
1-78
DDC

AFOSR-TR- 77 - 1286

STATE UNIVERSITY OF NEW YORK AT BUFFALO

LASER INDUCED THERMOELASTIC RESPONSE OF CIRCULAR PLATES

by

Herbert Reismann, Dennis P. Malone
and Peter S. Pawlik

Laboratory for Power and Environmental Studies

Faculty of
Engineering and
Applied Sciences

Qualified requestors may obtain additional copies from the Defense Documentation Center, all others should apply to the National Technical Information Service.

AIR FORCE OFFICE OF SCIENTIFIC RESEARCH (AFSC)
NOTICE OF TRANSMITTAL TO DDC
This technical report has been reviewed and is approved for public release IAW AFR 190-12 (7b).
Distribution is unlimited.
A. D. BLOSE
Technical Information Officer

UNCLASSIFIED

SECURITY CLASSIFICATION OF THIS PAGE (When Data Entered)

REPORT DOCUMENTATION PAGE	READ INSTRUCTIONS BEFORE COMPLETING FORM
1. REPORT NUMBER (19) (18) AFOSR-TR-77-1286	2. GOVT ACCESSION NO. / 3. RECIPIENT'S CATALOG NUMBER
4. TITLE (and Subtitle) (6) LASER INDUCED THERMOELASTIC RESPONSE OF CIRCULAR PLATES.	5. TYPE OF REPORT & PERIOD COVERED (9) INTERIM rept.,
	6. PERFORMING ORG. REPORT NUMBER
7. AUTHOR(S) (10) HERBERT REISMANN, DENNIS MALONE, PETER S PAWLIK	8. CONTRACT OR GRANT NUMBER(s) (15) AFOSR-76-2943
9. PERFORMING ORGANIZATION NAME AND ADDRESS STATE UNIVERSITY OF NEW YORK FACULTY OF ENGINEERING AND APPLIED SCIENCES BUFFALO, N Y 14214	10. PROGRAM ELEMENT, PROJECT, TASK AREA & WORK UNIT NUMBERS (16) 2307 (17) B1 61102F
11. CONTROLLING OFFICE NAME AND ADDRESS AIR FORCE OFFICE OF SCIENTIFIC RESEARCH/NA (11) BLDG 410 BOLLING AIR FORCE BASE, D C 20332	12. REPORT DATE Oct 77
	13. NUMBER OF PAGES 91 (12) 94p.
14. MONITORING AGENCY NAME & ADDRESS (if different from Controlling Office)	15. SECURITY CLASS. (of this report) UNCLASSIFIED
	15a. DECLASSIFICATION/DOWNGRADING SCHEDULE

16. DISTRIBUTION STATEMENT (of this Report)

Approved for public release; distribution unlimited.

17. DISTRIBUTION STATEMENT (of the abstract entered in Block 20, if different from Report)

18. SUPPLEMENTARY NOTES

19. KEY WORDS (Continue on reverse side if necessary and identify by block number)

SOLID MECHANICS
THERMOELASTIC PLATE THEORY
LASER INDUCED MOTION

20. ABSTRACT (Continue on reverse side if necessary and identify by block number)

A thermo-elastic model of a Laser irradiated plate is developed. The model accounts for plate flexure and shear deformation as well as plate stretching. An exact solution in series form is found for the dynamic response of a circular plate clamped at its boundary. The plate is subjected to Laser irradiation at its center, and normal to the plate surfaces. Experiments with a Holobeam model 630-Q Nd Laser were conducted to verify the mathematical model. A careful comparison between theory and experiment of transverse plate deflection induced by the Laser shows good agreement.

DD FORM 1 JAN 73 1473 EDITION OF 1 NOV 65 IS OBSOLETE

UNCLASSIFIED

SECURITY CLASSIFICATION OF THIS PAGE (When Data Entered)

405496

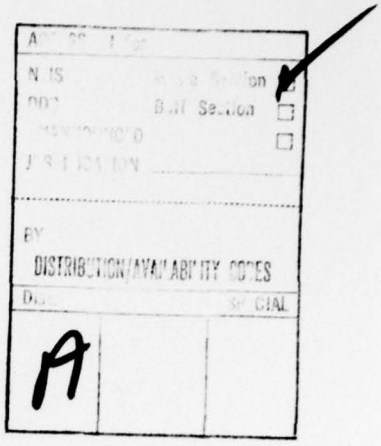

LASER INDUCED THERMOELASTIC RESPONSE OF CIRCULAR PLATES

by

Herbert Reismann,[1] Dennis P. Malone[1]

and Peter S. Pawlik[2]

Report No.

This research was supported by the
United States Air Force Office of Scientific Research
under Grant No. AF-AFOSR-76-2943

(1) Professor, State University of New York at Buffalo, N.Y. 14214, U.S.A.

(2) Associate Professor, State University of New York, College at Buffalo, N.Y. 14222, U.S.A.

TABLE OF CONTENTS

SUMMARY

A thermo-elastic model of a Laser irradiated plate is developed. The model accounts for plate flexure and shear deformation as well as plate stretching. An exact solution in series form is found for the dynamic response of a circular plate clamped at its boundary. The plate is subjected to Laser irradiation at its center, and normal to the plate surfaces. Experiments with a Holobeam model 630-Q Nd Laser were conducted to verify the mathematical model. A careful comparison between theory and experiment of transverse plate deflection induced by the Laser shows good agreement.

1.0 INTRODUCTION.

It is well known that Lasers have the inherent ability to deposit focused, radiant energy on a structure or its elements. Lasers can concentrate a short duration, high energy flux in an extremely narrow beam. The effect of short duration, high energy irradiation on an opaque solid can take several forms which are described (roughly) as follows (see Chapter 3 of ref. 5):

(a) Complete local vaporization of the material, and the resulting creation of openings (holes). If, in addition, the structure so punctured is in a state of initial stress, there will be an additional dynamic effect due to unloading waves and wave reflections, with the possibility of stress intensification.

(b) Sudden deposition of thermal energy, without a change in phase. This causes sudden thermal stresses in the structure, and because of the rapidity of the energy deposition process, there will be thermally generated stress waves.

(c) It is possible for the structure to experience partial surface vaporization over the effective Laser beam cross-section. This results in material removal and plasma generation. Subsequent heating of the plasma gives rise to shockwave formation, resulting in impulses transmitted to the solid.

Effects (a), (b), and (c) can coexist, but they can be separated for analytical purposes. The present analytical and experimental

investigation is concerned with case (b), above. We consider the specific case of a thin, circular plate, rigidly clamped at its boundary. The plate is subjected to Laser irradiation at its center, normal to the plate surface. The beam energy density is adjusted to cause heating of the plate, but to avoid phase changes (melting) of the plate material. Our objective is (a) to develop a mathematical model which predicts the thermoelastic dynamic response of the plate, and (b), to perform suitable experiments to establish the validity of the mathematical model.

2.0 THERMO-ELASTIC PLATE THEORY.

2.1 Plate Strain and Stress Components.

We shall derive a thermoelastic plate theory which accounts for stretching and bending of the plate. With regard to stretching, it is assumed that the plate stretches uniformly through the constant plate thickness h, with components $u_\alpha(x_1,x_2,t)$. With regard to plate bending, it is assumed that straight material elements (lines) originally normal to the plate median surface remain straight but rotate through an angle $\psi_\alpha(x_1,x_2,t)$. In the following, Greek subscripts take on the range 1,2; while Latin subscripts assume values 1,2,3. Thus the displacement vector $\tilde{u}_i$, i=1,2,3 assumes the form

$$\tilde{u}_\alpha(x_1,x_2,z,t) = z\psi_\alpha(x_1,x_2,t) + u_\alpha(x_1,x_2,t) \tag{1a}$$

$$\tilde{u}_z(x_1,x_2,z,t) = w(x_1,x_2,t) \tag{1b}$$

The general strain-displacement relation is

$$\varepsilon_{ij} = \frac{1}{2}(\tilde{u}_{i,j} + \tilde{u}_{j,i}) \tag{2}$$

and upon substitution of (1) into (2) we obtain

$$\begin{aligned} \varepsilon_{\alpha\beta} &= \frac{1}{2} z(\psi_{\alpha,\beta}+\psi_{\beta,\alpha}) + \frac{1}{2}(u_{\alpha,\beta}+ u_{\beta,\alpha}) \\ \varepsilon_{\alpha z} &= \varepsilon_{z\alpha} = \frac{1}{2}(\psi_\alpha + w_{,\alpha}); \quad \varepsilon_{zz} \equiv 0 \end{aligned} \tag{3}$$

It will be convenient to define the plate strain components

$$m_{\alpha\beta} = \frac{12}{h^3}\int_{-h/2}^{h/2} \varepsilon_{\alpha\beta} z dz = \frac{12}{h^3}\int_{-h/2}^{h/2} \varepsilon_{\beta\alpha} z dz = m_{\beta\alpha} \tag{4a}$$

$$q_\alpha = \frac{2}{h}\int_{-h/2}^{h/2} \varepsilon_{z\alpha}dz = \frac{2}{h}\int_{-h/2}^{h/2} \varepsilon_{\alpha z}dz \tag{4b}$$

$$n_{\alpha\beta} = \frac{1}{h}\int_{-h/2}^{h/2} \varepsilon_{\alpha\beta}dz = \frac{1}{h}\int_{-h/2}^{h/2} \varepsilon_{\beta\alpha}dz = n_{\beta\alpha} \tag{4c}$$

Similarly, we define the plate stress components by

$$M_{\alpha\beta} = \int_{-h/2}^{h/2} \tau_{\alpha\beta}zdz = \int_{-h/2}^{h/2} \tau_{\beta\alpha}zdz = M_{\beta\alpha} \tag{5a}$$

$$Q_\alpha = \int_{-h/2}^{h/2} \tau_{\alpha z}dz = \int_{-h/2}^{h/2} \tau_{z\alpha}dz \tag{5b}$$

$$N_{\alpha\beta} = \int_{-h/2}^{h/2} \tau_{\alpha\beta}dz = \int_{-h/2}^{h/2} \tau_{\beta\alpha}dz = N_{\beta\alpha} \tag{5c}$$

In view of (3) and (4), the plate strain-displacement relations are

$$m_{\alpha\beta} = \frac{1}{2}(\psi_{\alpha,\beta} + \psi_{\beta,\alpha}) \tag{6a}$$

$$q_\alpha = \psi_\alpha + w_{,\alpha} \tag{6b}$$

$$n_{\alpha\beta} = \frac{1}{2}(u_{\alpha,\beta} + u_{\beta,\alpha}) \tag{6c}$$

and we note that

$$\varepsilon_{\alpha\beta} = zm_{\alpha\beta} + n_{\alpha\beta} \quad , \quad \varepsilon_{\alpha z} = \varepsilon_{z\alpha} = \frac{1}{2}q_\alpha \tag{7}$$

2.2 Stress Equations of Motion.

We shall now derive the pertinent equations of motion with the aid of Hamilton's principle

$$\int_{t_1}^{t_2} (\delta K - \delta U + \delta W)dt = 0 \tag{8}$$

where δK and δU are the first variations of kinetic and potential energy in the plate, respectively, and δW is the virtual work of external forces in an (admissible) variation of the plate displacement field. The kinetic energy of a solid with volume V is given by

$$K = \frac{1}{2}\int_V \rho\dot{\tilde{u}}_i\dot{\tilde{u}}_i\, dV = \frac{1}{2}\int_V \rho(\dot{\tilde{u}}_1^2 + \dot{\tilde{u}}_2^2 + \dot{\tilde{u}}_3^2)dV \tag{9}$$

With reference to (1) we have

$$\dot{\tilde{u}}_\alpha = z\dot{\psi}_\alpha + \dot{u}_\alpha \quad , \quad \dot{\tilde{u}}_3 = \dot{w} \tag{10}$$

and upon substitution of (10) into (9), we obtain

$$K = \frac{1}{2}\int_A \int_{-h/2}^{h/2} \rho(z^2\dot{\psi}_\alpha\dot{\psi}_\alpha + \dot{w}^2 + \dot{u}_\alpha\dot{u}_\alpha + 2z\dot{u}_\alpha\dot{\psi}_\alpha)dz\, dA$$

$$= \frac{1}{2}\int_A (\rho h\dot{w}^2 + \frac{1}{12}\rho h^3\dot{\psi}_\alpha\dot{\psi}_\alpha + \rho h\dot{u}_\alpha\dot{u}_\alpha)dA \tag{11}$$

Taking the first variation of (11) with respect to displacements,

$$\delta K = \int_A (\rho h\dot{w}\delta\dot{w} + \frac{1}{12}\rho h^3\dot{\psi}_\alpha\delta\dot{\psi}_\alpha + \rho h\dot{u}_\alpha\delta\dot{u}_\alpha)dA \tag{12}$$

We now integrate both sides of (12) with respect to time from t_1 to t_2, and then use integration by parts on the right hand side. In line with the requirements of Hamilton's principle, we set $\delta\psi_\alpha = \delta w = \delta u_\alpha = 0$ at $t=t_1$ and at $t=t_2$. Thus we obtain the result

$$\int_{t_1}^{t_2} \delta K dt = -\int_{t_1}^{t_2}\int_A (\rho h\ddot{w}\delta w + \frac{1}{12}\rho h^3\ddot{\psi}_\alpha\delta\psi_\alpha + \rho h\ddot{u}_\alpha\delta u_\alpha)dA dt \tag{13}$$

The variation of the strain energy density of the plate is given by (see (37))

$$\delta \mathcal{W}_p = M_{\alpha\beta}\delta m_{\alpha\beta} + Q_\alpha \delta q_\alpha + N_{\alpha\beta}\delta n_{\alpha\beta} \tag{14}$$

Consequently, the variation of the total strain energy is given by

$$\begin{aligned}\delta U &= \int_A \delta \mathcal{W}_p dA = \int_A (M_{\alpha\beta}\delta m_{\alpha\beta} + Q_\alpha \delta q_\alpha + N_{\alpha\beta}\delta n_{\alpha\beta})dA \\ &= \int_A (M_{\alpha\beta}\delta\psi_{\alpha,\beta} + Q_\alpha \delta\psi_\alpha + Q_\alpha \delta w_{,\alpha} + N_{\alpha\beta}\delta u_{\alpha,\beta})dA \end{aligned} \tag{15}$$

where we have used (6). Upon application of Green's theorem in the plane to (15), we obtain

$$\begin{aligned}\delta U = &\oint_C (M_{\alpha\beta}\delta\psi_\alpha n_\beta + Q_\alpha \delta w n_\alpha + N_{\alpha\beta}\delta u_\alpha n_\beta)d\ell \\ &-\int_A [(M_{\alpha\beta,\beta} - Q_\alpha)\delta\psi_\alpha + Q_{\alpha,\alpha}\delta w + N_{\alpha\beta,\beta}\delta u_\alpha]dA \end{aligned} \tag{16}$$

where C is the boundary curve of the simply connected domain of the plate, and $\hat{n}, \hat{\ell}$ are unit vectors which are normal and tangential, respectively, to C. We also note the relationships

$$\left.\begin{aligned} u_n &= n_\alpha u_\alpha & u_\ell &= \ell_\alpha u_\alpha \\ \psi_n &= n_\alpha \psi_\alpha & \psi_\ell &= \ell_\alpha \psi_\alpha \\ Q_n &= n_\alpha Q_\alpha & Q_\ell &= Q_\alpha \ell_\alpha \\ M_{nn} &= n_\alpha n_\beta M_{\alpha\beta} & M_{n\ell} &= \ell_\alpha n_\beta M_{\alpha\beta} \\ N_{nn} &= n_\alpha n_\beta N_{\alpha\beta} & N_{n\ell} &= \ell_\alpha n_\beta N_{\alpha\beta} \end{aligned}\right\} \tag{17}$$

and

$$\left.\begin{aligned} M_{\alpha\beta}\delta\psi_\alpha n_\beta &= M_{nn}\delta\psi_n + M_{n\ell}\delta\psi_\ell \\ N_{\alpha\beta}\delta u_\alpha n_\beta &= N_{nn}\delta u_n + N_{n\ell}\delta u_\ell \end{aligned}\right\} \tag{18}$$

It can be shown (p. 465, eq. (14.19), ref. [1]) that the virtual work of external applied forces and boundary forces is given by

$$\delta W = \int_A p\delta w dA + \oint_C (M^*_{nn}\delta\psi_n + M^*_{n\ell}\delta\psi_\ell + Q^*_n\delta w + N^*_{nn}\delta u_n + N^*_{n\ell}\delta u_\ell)d\ell \tag{19}$$

where p is the transverse, normal pressure acting on the plate in A and M^*_{nn}, Q^*_n, etc., are stress resultants acting on the boundary C. Upon substitution of (13), (16), and (19) into (8) we obtain

$$\begin{aligned}\int_{t_1}^{t_2}\int_A [&(-\rho h\ddot{w}+Q_{\alpha,\alpha}+p)\delta w+(-\tfrac{1}{12}\rho h^3\ddot{\psi}_\alpha+M_{\alpha\beta,\beta}-Q_\alpha)\delta\psi_\alpha \\ &+(-\rho h\ddot{u}_\alpha+N_{\alpha\beta,\beta})\delta u_\alpha]dA \\ &+\int_{t_1}^{t_2}\oint_C [(M^*_{nn}-M_{nn})\delta\psi_n+(M^*_{n\ell}-M_{n\ell})\delta\psi_\ell+(Q^*_n-Q_n)\delta w \\ &+(N^*_{n\ell}-N_{n\ell})\delta u_\ell+(N^*_{nn}-N_{nn})\delta u_n]d\ell dt = 0\end{aligned} \tag{20}$$

Since A, C and t_2-t_1 are arbitrary, the two integrals in (20) vanish separately. Furthermore, the displacement variations are arbitrary in A and on that portion of C where stress resultants are prescribed. We thus infer that in A

$$-\rho h\ddot{w} + Q_{\alpha,\alpha} + p = 0 \tag{21a}$$

$$-\tfrac{1}{12}\rho h^3\ddot{\psi}_\alpha + M_{\alpha\beta,\beta} - Q_\alpha = 0 \tag{21b}$$

$$-\rho h\ddot{u}_\alpha + N_{\alpha\beta,\beta} = 0 \tag{21c}$$

and on C one member of each of the following pairs is specified:

$$(w,\ Q_n),\qquad (\psi_n,\ M_{nn}),\qquad (\psi_\ell,\ M_{n\ell}) \tag{22a}$$

$$(u_n,\ N_{nn}),\qquad (u_\ell,\ N_{n\ell}) \tag{22b}$$

2.3 Constitutive Relations and Displacement Equations of Motion.

We assume that the Neumann-Duhamel relation expresses the relation between stress, strain, and temperature in a homogeneous, isotropic material, i.e.,

$$E\varepsilon_{ij} = (1+\nu)\tau_{ij} - \nu\tau_{kk}\delta_{ij} + E\alpha T\delta_{ij} \tag{23}$$

For our present purpose we write

$$E\varepsilon_{\alpha\beta} = (1+\nu)\tau_{\alpha\beta} - \nu\tau_{\gamma\gamma}\delta_{\alpha\beta} - \nu\tau_{zz}\delta_{\alpha\beta} + E\alpha T\delta_{\alpha\beta} \tag{24a}$$

$$\tau_{z\alpha} = 2\kappa^2 G\varepsilon_{z\alpha} \tag{24b}$$

and we ignore the relation

$$E\varepsilon_{zz} = \tau_{zz} - \nu\tau_{\gamma\gamma} + E\alpha T = 0 \tag{24c}$$

If we set $\alpha=\beta$ in (24a), we obtain

$$\tau_{\alpha\alpha} = \frac{E}{(1-\nu)}\varepsilon_{\alpha\alpha} + \frac{2\nu}{(1-\nu)}\tau_{zz} - \frac{2E\alpha T}{(1-\nu)} \tag{25}$$

and therefore

$$\tau_{\alpha\beta} = \frac{E}{(1+\nu)}\varepsilon_{\alpha\beta} + \frac{\nu E}{(1-\nu^2)}\varepsilon_{\gamma\gamma}\delta_{\alpha\beta} + \frac{\nu}{1-\nu}\tau_{zz}\delta_{\alpha\beta} - \frac{E\alpha T}{1-\nu}\delta_{\alpha\beta} \tag{26}$$

Upon substitution of (26) into (5) and application of (4), we readily obtain

$$M_{\alpha\beta} = D[(1-\nu)m_{\alpha\beta}+\nu m\delta_{\alpha\beta}] - \frac{M_T}{(1-\nu)}\delta_{\alpha\beta} + \frac{\nu\delta_{\alpha\beta}}{(1-\nu)}\int_{-h/2}^{h/2} z\tau_{zz}dz \tag{27a}$$

A similar calculation reveals that

$$N_{\alpha\beta} = \frac{Eh}{(1-\nu^2)}[(1-\nu)n_{\alpha\beta}+\nu n\delta_{\alpha\beta}] - \frac{N_T\delta_{\alpha\beta}}{(1-\nu)} + \frac{\nu\delta_{\alpha\beta}}{(1-\nu)}\int_{-h/2}^{h/2}\tau_{zz}dz \tag{27b}$$

$$Q_\alpha = \kappa^2 Ghq_\alpha \tag{27c}$$

where

$$m = m_{\alpha\alpha} = \psi_{\alpha,\alpha} = \vec{\nabla}\cdot\vec{\psi} \qquad M_T = \alpha E \int_{-h/2}^{h/2} zT\,dz$$

$$n = n_{\alpha\alpha} = u_{\alpha,\alpha} = \vec{\nabla}\cdot\vec{u} \qquad N_T = \alpha E \int_{-h/2}^{h/2} T\,dz \tag{28}$$

We now drop (neglect) the integrals in (27a) and (27b). Thus we obtain the plate stress-strain relations:

$$N_{\alpha\beta} = \frac{Eh}{(1-\nu^2)}\left[(1-\nu)n_{\alpha\beta} + \nu n\delta_{\alpha\beta}\right] - \frac{N_T}{(1-\nu)}\delta_{\alpha\beta} \tag{29a}$$

$$M_{\alpha\beta} = D\left[(1-\nu)m_{\alpha\beta} + \nu m\delta_{\alpha\beta}\right] - \frac{M_T}{(1-\nu)}\delta_{\alpha\beta} \tag{29b}$$

$$Q_\alpha = Ghq_\alpha \tag{29c}$$

Upon substitution of (6) into (29), we obtain the plate stress-displacement relations

$$N_{\alpha\beta} = \frac{Eh}{2(1-\nu^2)}\left[(1-\nu)(u_{\alpha,\beta} + u_{\beta,\alpha}) + 2\nu u_{\gamma,\gamma}\delta_{\alpha\beta}\right] - \frac{N_T\delta_{\alpha\beta}}{(1-\nu)} \tag{30a}$$

$$M_{\alpha\beta} = \frac{1}{2}D\left[(1-\nu)(\psi_{\alpha,\beta} + \psi_{\beta,\alpha}) + 2\nu\psi_{\gamma,\gamma}\delta_{\alpha\beta}\right] - \frac{M_T\delta_{\alpha\beta}}{(1-\nu)} \tag{30b}$$

$$Q_\alpha = \kappa^2 Gh(\psi_\alpha + w_{,\alpha}) \tag{30c}$$

Further substitution of (30) into (21) results in the displacement equations of motion for the plate:

$$\rho h\ddot{u}_\alpha = \frac{Eh}{2(1-\nu^2)}\left[(1-\nu)u_{\alpha,\beta\beta} + (1+\nu)u_{\beta,\beta\alpha}\right] - \frac{(N_T)_{,\alpha}}{(1-\nu)} \tag{31a}$$

$$\frac{1}{12}\rho h^3\ddot{\psi}_\alpha = \frac{1}{2}D\left[(1-\nu)\psi_{\alpha,\beta\beta} + (1+\nu)\psi_{\beta,\beta\alpha}\right] - \kappa^2 Gh(\psi_\alpha + w_{,\alpha}) - \frac{(M_T)_{,\alpha}}{(1-\nu)} \tag{31b}$$

$$\rho h\ddot{w} = \kappa^2 Gh(\psi_{\alpha,\alpha} + w_{,\alpha\alpha}) + p \tag{31c}$$

Equation (30) can also be written in (invariant) vector form:

$$\rho h\ddot{\vec{u}} = \frac{Eh}{2(1-\nu^2)}\left[(1-\nu)\nabla^2\vec{u} + (1+\nu)\vec{\nabla}(\vec{\nabla}\cdot\vec{u})\right] - \frac{\vec{\nabla}(N_T)}{(1-\nu)} \tag{31a}$$

$$\frac{1}{12}\rho h^3\ddot{\vec{\psi}} = \frac{1}{2}D\left[(1-\nu)\nabla^2\vec{\psi} + (1+\nu)\vec{\nabla}(\vec{\nabla}\cdot\vec{\psi})\right] - \kappa^2 Gh(\vec{\psi}+\vec{\nabla}w) - \frac{\vec{\nabla}(M_T)}{(1-\nu)} \tag{31b}$$

$$\rho h\ddot{w} = \kappa^2 Gh(\vec{\nabla}\cdot\vec{\psi} + \nabla^2 w) + p \tag{31c}$$

2.4 Energy Considerations

In general, the time rate of change of strain energy density is given by $\dot{W} = \tau_{ij}\dot{\varepsilon}_{ij}$ (see p. 267 of ref. [1]). For the plate, this can be expressed as $\tau_{ij}\dot{\varepsilon}_{ij} = \tau_{\alpha\beta}(z\dot{m}_{\alpha\beta}+\dot{n}_{\alpha\beta})+\tau_{\alpha z}\dot{q}_{\alpha}$. Consequently, the time rate of change of strain energy per unit area of plate is

$$\dot{W}_p = \int_{-h/2}^{h/2} [\tau_{\alpha\beta}(z\dot{m}_{\alpha\beta}+\dot{n}_{\alpha\beta}) + \tau_{\alpha z}\dot{q}_{\alpha}]dz$$

$$= M_{\alpha\beta}\dot{m}_{\alpha\beta} + Q_{\alpha}\dot{q}_{\alpha} + N_{\alpha\beta}\dot{n}_{\alpha\beta} \tag{32}$$

where we have used (5). However,

$$\dot{W}_p = \frac{\partial W_p}{\partial m_{\alpha\beta}}\,\dot{m}_{\alpha\beta} + \frac{\partial W_p}{\partial q_{\alpha}}\,\dot{q}_{\alpha} + \frac{\partial W_p}{\partial n_{\alpha\beta}}\,\dot{n}_{\alpha\beta} \tag{33}$$

and combining (32) and (33), we obtain

$$\left(\frac{\partial W_p}{\partial m_{\alpha\beta}} - M_{\alpha\beta}\right)\dot{m}_{\alpha\beta} + \left(\frac{\partial W_p}{\partial q_{\alpha}} - Q_{\alpha}\right)\dot{q}_{\alpha} + \left(\frac{\partial W_p}{\partial n_{\alpha\beta}} - N_{\alpha\beta}\right)\dot{n}_{\alpha\beta}=0 \tag{34}$$

This result must be valid for all processes, i.e., $\dot{m}_{\alpha\beta}$, $\dot{q}_{\alpha}$, and $\dot{n}_{\alpha\beta}$ are arbitrary. We thus conclude that

$$M_{\alpha\beta} = \frac{\partial W_p}{\partial m_{\alpha\beta}}, \qquad Q_{\alpha} = \frac{\partial W_p}{\partial q_{\alpha}}, \qquad N_{\alpha\beta} = \frac{\partial W_p}{\partial n_{\alpha\beta}} \tag{35}$$

and it is evident that the scalar function $W_p = W_p(m_{11}, m_{12}, m_{22}, q_1, q_2, n_{11}, n_{12}, n_{22})$ completely characterizes the mechanical configuration of the homogeneous plate. In view of (35) and (29), the pertinent strain energy density function for the plate is given by

$$2\mathcal{W}_p = D(1-\nu)m_{\alpha\beta}m_{\alpha\beta} + D\nu m^2 - \frac{2M_T}{(1-\nu)}\,m + \frac{Eh}{(1+\nu)}\,n_{\alpha\beta}\,n_{\alpha\beta} + \frac{Eh\nu m^2}{(1-\nu^2)}$$

$$- \frac{2N_T}{(1-\nu)}\,n + \kappa^2 Ghq_\alpha q_\alpha \tag{36}$$

With reference to (36) and (29), we also note that

$$\delta\mathcal{W}_p = M_{\alpha\beta}\delta m_{\alpha\beta} + Q_\alpha \delta q_\alpha + N_{\alpha\beta}\delta n_{\alpha\beta} \tag{37}$$

and this result was used in (15).

2.5 Reduction to Classical Plate Theory.

If we neglect rotatory inertia in (21), i.e., if $\frac{1}{12}\rho h^3\ddot{\psi}_\alpha = 0$, then the stress equations of motion reduce to

$$Q_{\alpha,\alpha} + p = \rho h\ddot{w}, \qquad Q_\alpha = M_{\alpha\beta,\beta}$$

or

$$M_{\alpha\beta,\beta\alpha} + p = \rho h\ddot{w} \tag{38}$$

In classical plate theory it is assumed that material line elements originally normal to the median surface remain normal during deformation, i.e., $\psi_\alpha = -w_{,\alpha}$. Consequently $m_{\alpha\beta} = w_{,\alpha\beta}$ and $q_\alpha = 0$, i.e., the plate is rigid with respect to shearing deformations. In this case

$$M_{\alpha\beta} = -D[(1-\nu)w_{,\alpha\beta} + \nu(\nabla^2 w)\delta_{\alpha\beta}] - \frac{M_T}{(1-\nu)}\,\delta_{\alpha\beta} \tag{39a}$$

$$Q_\alpha = M_{\alpha\beta,\beta} = -D(\nabla^2 w)_{,\alpha} - \frac{(M_T)_{,\alpha}}{(1-\nu)} \tag{39b}$$

or

$$\vec{Q} = -D\vec{\nabla}(\nabla^2 w) - \frac{1}{(1-\nu)}\vec{\nabla}(M_T) \tag{39b}$$

Upon substitution of (39) into (38), we obtain

$$\rho h\ddot{w} + D\nabla^4 w = p - \frac{1}{(1-\nu)}\nabla^2 M_T \tag{40}$$

Equation (40) is the well known equation of a plate within the framework of classical plate theory, including thermal (bending) terms (see [2], p. 384, eq. (12.2.15)).

3.0 RESOLUTION OF BOUNDARY VALUE PROBLEMS.

3.1 Generalities

Inspection of equations (31) and (22) reveals that the plate stretching problem can be decoupled from the plate bending problem in the present formulation. In the present section we shall present a formal solution for each of these problems. We shall use the method of Williams (a modified eigenfunction technique) to obtain a solution. Since the present approach is a generalization of a technique developed in reference [1], we shall present only the final results, omitting most of the details.

3.2 Plane Extensional Motion.

The problem is characterized by (21c), (22b), and (30a), i.e.,

$$-\rho h \ddot{u}_\alpha + N_{\alpha\beta,\beta} = 0 \text{ in } A \tag{41a}$$

where

$$N_{\alpha\beta} = \frac{Eh}{2(1-\nu^2)} [(1-\nu)(u_{\alpha,\beta}+u_{\beta,\alpha})+2\nu u_{\gamma,\gamma}\delta_{\alpha\beta}] - \frac{N_T \delta_{\alpha\beta}}{(1-\nu)} \tag{41b}$$

and

$$(u_n \text{ or } N_{nn}) \text{ and } (u_\ell \text{ or } N_{n\ell}) \tag{41c}$$

are specified on C. For a unique solution, we adjoin the initial conditions

$$u_\alpha(x_1,x_2,0) = u_\alpha^o, \; \dot{u}_\alpha(x_1,x_2,0) = \dot{u}_\alpha^o \tag{41d}$$

The solution of the problem characterized in (41) is given by

$$u_\alpha(x_1,x_2,t) = u_\alpha^{(s)}(x_1,x_2,t) + \sum_{i=1}^{\infty} u_\alpha^{(i)}(x_1,x_2)q_i(t) \tag{42a}$$

$$N_{\alpha\beta}(x_1,x_2,t) = N^{(s)}_{\alpha\beta}(x_1,x_2,t) + \sum_{i=1}^{\infty} N^{(i)}_{\alpha\beta}(x_1,x_2)q_i(t) \tag{42b}$$

The terms of the solution (42) which carry the superscript (s) are obtained from the quasi-static problem

$$N^{(s)}_{\alpha\beta,\beta}=0 \qquad \text{in A} \tag{43a}$$

$$N^{(s)}_{\alpha\beta} = \frac{Eh}{2(1-\nu^2)}\left[(1-\nu)(u^{(s)}_{\alpha,\beta}+u^{(s)}_{\beta,\alpha})+2\nu u^{(s)}_{\gamma,\gamma}\delta_{\alpha\beta}\right] - \frac{N_T\delta_{\alpha\beta}}{(1-\nu)} \tag{43b}$$

and

$$\left.\begin{array}{l}(u^{(s)}_n \text{ or } N^{(s)}_{nn}) \quad \text{and} \quad (u^{(s)}_\ell \text{ and } N^{(s)}_{n\ell}) \text{ are} \\ \text{specified on C as in (41c)}\end{array}\right\} \tag{43c}$$

Quantities in (42) which carry the superscript (i) are associated with the eigenfunctions characterized by the homogeneous equations

$$N^{(i)}_{\alpha\beta,\beta} = -\rho h\omega_i^2 u^{(i)}_\alpha \qquad \text{in A} \tag{44a}$$

$$N^{(i)}_{\alpha\beta} = \frac{Eh}{2(1-\nu^2)}\left[(1-\nu)(u^{(i)}_{\alpha,\beta}+u^{(i)}_{\beta,\alpha}) + 2\nu u^{(i)}_{\gamma,\gamma}\delta_{\alpha\beta}\right] \tag{44b}$$

$$(u^{(i)}_n \text{ or } N^{(i)}_{nn}=0) \text{ and } (u^{(i)}_\ell \text{ or } N^{(i)}_{n\ell}=0) \text{ on C} \tag{44c}$$

The eigenfunctions satisfy the orthonormality relation

$$\int_A \rho h u^{(i)}_\alpha u^{(j)}_\alpha dA = \delta_{ij} \tag{44d}$$

With the above definition, it can be shown that

$$q_i(t) = [q_i(o)-Q_i(o)]\cos\omega_i t + \frac{1}{\omega_i}[\dot{q}_i(o)-\dot{Q}_i(o)]\sin\omega_i t + Q_i(t)-\omega_i\int_o^t Q_i(\tau)\sin\omega_i(t-\tau)d\tau \tag{45}$$

where

$$\omega_i^2 Q_i(t) = -\int_A \frac{N_T}{(1-\nu)} u_{\alpha,\alpha}^{(i)} dA + \oint_C (u_n^{(s)} N_{nn}^{(i)} - u_n^{(i)} N_{nn}^{(s)} + u_\ell^{(s)} N_{n\ell}^{(i)} - u_\ell^{(i)} N_{n\ell}^{(s)}) d\ell \tag{46a}$$

and

$$q_i(o) - Q_i(o) = \int_A \rho h u_\alpha^{(i)} u_\alpha^{(o)} dA \tag{46b}$$

$$\dot{q}_i(o) - \dot{Q}_i(o) = \int_A \rho h \dot{u}_\alpha^{(i)} \dot{u}_\alpha^{(o)} dA \tag{46c}$$

3.3 Bending (Flexural) Motion.

In this case the problem is stated by (21a), (21b), (22a), (30b) and (30c), i.e.,

$$-\rho h \ddot{w} + Q_{\alpha,\alpha} + p = 0 \tag{47a}$$

$$-\frac{1}{12} \rho h^3 \ddot{\psi}_\alpha + M_{\alpha\beta,\beta} - Q_\alpha = 0 \tag{47b}$$

where

$$Q_\alpha = \kappa^2 G h (\psi_\alpha + w_{,\alpha}) \tag{47c}$$

$$M_{\alpha\beta} = \frac{1}{2} D [(1-\nu)(\psi_{\alpha,\beta} + \psi_{\beta,\alpha}) + 2\nu \psi_{\gamma,\gamma} \delta_{\alpha\beta}] - \frac{M_T \delta_{\alpha\beta}}{(1-\nu)} \tag{47d}$$

and

$$(\psi_n \text{ or } M_{nn}), \quad (\psi_\ell \text{ or } M_{n\ell}) \text{ and } (w \text{ or } Q_n) \tag{47e}$$

are specified on C. For a unique solution, we adjoin the initial conditions

$$\begin{aligned} w(x_1, x_2, 0) &= w^{(o)} \quad ; \quad \psi_\alpha(x_1, x_2, 0) = \psi_\alpha^{(o)} \\ \dot{w}(x_1, x_2, 0) &= \dot{w}^{(o)} \quad ; \quad \dot{\psi}_\alpha(x_1, x_2, 0) = \dot{\psi}_\alpha^{(o)} \end{aligned} \tag{47f}$$

The solution of the problem characterized by (47) is given by

$$w(x_1,x_2,t) = w^{(s)}(x_1,x_2,t) + \sum_{i=1}^{\infty} w^{(i)}(x_1,x_2)q_i(t) \tag{48a}$$

$$\psi_\alpha(x_1,x_2,t) = \psi_\alpha^{(s)}(x_1,x_2,t) + \sum_{i=1}^{\infty} \psi_\alpha^{(i)}(x_1,x_2)q_i(t) \tag{48b}$$

$$Q_\alpha(x_1,x_2,t) = Q_\alpha^{(s)}(x_1,x_2,t) + \sum_{i=1}^{\infty} Q_\alpha^{(i)}(x_1,x_2)q_i(t) \tag{48c}$$

$$M_{\alpha\beta}(x_1,x_2,t) = M_{\alpha\beta}^{(s)}(x_1,x_2,t) + \sum_{i=1}^{\infty} M_{\alpha\beta}^{(i)}(x_1,x_2)q_i(t) \tag{48d}$$

The terms of the solution (48) which carry the superscript (s) are obtained from the quasi static problem

$$Q_{\alpha,\alpha}^{(s)} + p = 0 \qquad \text{in A} \tag{49a}$$

$$M_{\alpha\beta,\beta}^{(s)} - Q_\alpha^{(s)} = 0 \tag{49b}$$

where

$$Q_\alpha^{(s)} = \kappa^2 Gh(\psi_\alpha^{(s)} + w_{,\alpha}^{(s)}) \tag{49c}$$

$$M_{\alpha\beta}^{(s)} = \frac{1}{2} D\left[(1-\nu)(\psi_{\alpha,\beta}^{(s)} + \psi_{\beta,\alpha}^{(s)}) + 2\nu\psi_{\gamma,\gamma}^{(s)}\delta_{\alpha\beta}\right] - \frac{M_T}{(1-\nu)}\delta_{\alpha\beta} \tag{49d}$$

and

$$(\psi_n^{(s)} \text{ or } M_{nn}^{(s)}), \quad (\psi_\ell^{(s)} \text{ or } M_{n\ell}^{(s)}) \text{ and } (w^{(s)} \text{ or } Q_n^{(s)}) \tag{49e}$$

are specified on C as in (47e). Quantities in (48) which carry the superscript (i) are associated with the eigenfunctions characterized by the homogeneous equations

$$\left.\begin{aligned} Q_{\alpha,\alpha}^{(i)} &= -\rho h\omega_i^2 w^{(i)} \qquad (50a)\\ M_{\alpha\beta,\beta}^{(i)} - Q_\alpha^{(i)} &= -\rho\frac{h^3}{12}\omega_i^2\psi_\alpha^{(i)} \qquad (50b)\end{aligned}\right\} \quad \text{in A}$$

$$(w^{(i)} \text{ or } Q_n^{(i)}=0), \quad (\psi_n^{(i)} \text{ or } M_{nn}^{(i)}=0), \text{ and } (\psi_\ell^{(i)} \text{ or } M_{n\ell}^{(i)}=0) \tag{50c}$$

on C.

The eigenfunctions satisfy the orthonormality relations

$$\int_A (\rho h w^{(i)} w^{(j)} + \rho \frac{h^3}{12} \psi_\alpha^{(i)} \psi_\alpha^{(j)}) dA = \delta_{ij} \tag{50d}$$

In this case it can be shown that $q_i(t)$ is again defined by (45), and in this case

$$\omega_i^2 Q_i(t) = \oint_C (w^{(s)} Q_n^{(i)} - w^{(i)} Q_n^{(s)} + \psi_n^{(s)} M_{nn}^{(i)} - \psi_n^{(i)} M_{nn}^{(s)} + \psi_\ell^{(s)} M_{n\ell}^{(i)} - \psi_\ell^{(i)} M_{n\ell}^{(s)}) dA - \int_A (w^{(i)} p + \frac{M_T}{(1-\nu)} \psi_{\alpha,\alpha}^{(i)}) dA \tag{51a}$$

$$q_i(o) - Q_i(o) = \int_A (\rho h w^{(o)} w^{(i)} + \rho \frac{h^3}{12} \psi_\alpha^{(o)} \psi_\alpha^{(i)}) dA \tag{51b}$$

$$\dot{q}_i(o) - \dot{Q}_i(o) = \int_A (\rho h \dot{w}^{(o)} w^{(i)} + \rho \frac{h^3}{12} \dot{\psi}_\alpha^{(o)} \psi_\alpha^{(i)}) dA \tag{51c}$$

In the following we shall consider the special case of a circular plate with radius a which is rigidly clamped at its boundary. The plate will be subjected to laser irradiation at its center, i.e., the excitation as well as the response of the plate will be axisymmetric. In addition, it will be assumed that the plate is at rest and in a state of static equilibrium at t=0. For these reasons we now write the principal equation in axisymmetric polar coordinates with the pole at the center of the plate. Consequently we have

(a) Plate Stretching:

$$u_r \equiv u(r,t), \quad u_\theta \equiv 0 \tag{52a}$$

$$-\rho h\ddot{u} + \frac{\partial N_{rr}}{\partial r} + \frac{1}{r}(N_{rr}-N_{\theta\theta}) = 0 \tag{52b}$$

$$\left.\begin{aligned} N_{rr} &= \frac{Eh}{1-\nu^2}\left(\frac{\partial u}{\partial r} + \frac{\nu}{r}u\right) - \frac{N_T}{1-\nu} \\ N_{\theta\theta} &= \frac{Eh}{1-\nu^2}\left(\nu\frac{\partial u}{\partial r} + \frac{1}{r}u\right) - \frac{N_T}{1-\nu} \end{aligned}\right\} \tag{52c}$$

$$u(a,t) = 0 \tag{52d}$$

$$u(r,o) = 0, \qquad \dot{u}(r,o) = 0 \tag{52e}$$

$$\left.\begin{aligned} u(r,t) &= u^{(s)}(r,t) + \sum_{i=1}^{\infty} u^{(i)}(r)\cdot q_i(t) \\ N_{rr}(r,t) &= N_{rr}^{(s)}(r,t) + \sum_{i=1}^{\infty} N_{rr}^{(i)}(r)\cdot q_i(t) \\ N_{\theta\theta}(r,t) &= N_{\theta\theta}^{(s)}(r,t) + \sum_{i=1}^{\infty} N_{\theta\theta}^{(i)}(r)\cdot q_i(t) \end{aligned}\right\} \tag{53}$$

$$\left.\begin{aligned} \omega_i^2 Q_i(t) &= -\frac{2\pi}{(1-\nu)}\int_o^a N_T\frac{\partial}{\partial r}(ru^{(i)})dr \\ q_i(t) &= Q_i(t) - \omega_i\int_o^t Q_i(\tau)\sin\omega_i(t-\tau)d\tau \end{aligned}\right\} \tag{54}$$

(b) Plate Bending

$$\left.\begin{aligned} -\rho h\ddot{w} + \frac{\partial Q_r}{\partial r} + \frac{Q_r}{r} &= 0 \\ -\frac{\rho h^3}{12}\ddot{\psi} + \frac{\partial M_{rr}}{\partial r} + \frac{1}{r}(M_{rr}-M_{\theta\theta}) - Q_r &= 0 \end{aligned}\right\} \tag{55a}$$

$$\left.\begin{aligned} M_{rr} &= D\left(\frac{\partial\psi}{\partial r} + \frac{\nu}{r}\psi\right) - \frac{M_T}{1-\nu} \\ M_{\theta\theta} &= D\left(\nu\frac{\partial\psi}{\partial r} + \frac{1}{r}\psi\right) - \frac{M_T}{1-\nu} \\ Q_r &= \kappa^2 Gh\left(\psi + \frac{\partial w}{\partial r}\right) \end{aligned}\right\} \tag{55b}$$

$$\psi(a,t) = w(a,t) = 0 \tag{55c}$$

$$w(r,0) = \dot{w}(r,0) = 0, \qquad \psi(r,0) = \dot{\psi}(r,0) = 0 \tag{55d}$$

$$\left.\begin{aligned} w(r,t) &= w^{(s)}(r,t) + \sum_{i=1}^{\infty} w^{(i)}(r) q_i(t) \\ \psi(r,t) &= \psi^{(s)}(r,t) + \sum_{i=1}^{\infty} \psi^{(i)}(r) q_i(t) \end{aligned}\right\} \tag{56}$$

$$\left.\begin{aligned} \omega_i^2 Q_i(t) &= -\frac{2\pi}{1-\nu} \int_0^a M_T \frac{\partial}{\partial r}(r\psi^{(i)})\,dr \\ q_i(t) &= Q_i(t) - \omega_i \int_0^t Q_i(\tau) \sin \omega_i (t-\tau)\,d\tau \end{aligned}\right\} \tag{57}$$

4.0 LASER INDUCED HEATING OF THE PLATE

4.1 Temperature Distribution in the Plate

In order to obtain a mathematical model of the temperature distribution induced in the plate by a pulsed laser, several assumptions will be made. These assumptions yield a model which is both physically realistic and mathematically tractable in the forthcoming analysis. The geometries of the clamped circular plate and of the laser irradiance are shown in Fig. 1. With reference to the dimensions shown in Fig. 1, the five basic assumptions are as follows:

(A-1) The laser irradiance is spacially axisymmetric with a Gaussian distribution of the form $\exp[-(r/d)^2]$ where d, which is called the laser spot size, is the radial distance at which the incident irradiance has decreased to 1/e of its maximum value I_m.

(A-2) The laser irradiance also has a Gaussian distribution in time of the form $\exp[-(t/\tau)^2]$ where τ, which is called the pulse duration, is the time required for the incident irradiance to decrease to 1/e of its initial value.

(A-3) The radius of the plate is essentially infinite compared to the laser spot size, i.e., $a/d \gg 1$.

(A-4) The plate is sufficiently thick so that, for the time interval of interest, the temperature rise of the back surface does not have an appreciable effect on the motion. This condition is difficult to express analytically, however one rough approximation is obtained from the inequality $h^2/4Kt_p > 1$. Here h is the plate thickness, K is the thermal diffusivity of the plate and t_p is a characteristic time, e.g., the fundamental period

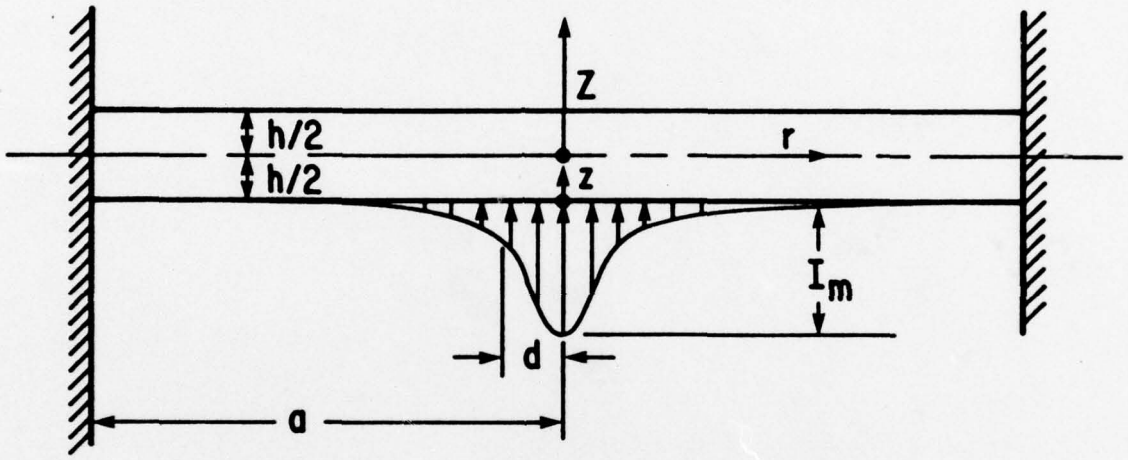

Figure 1: Geometry of Plate and Laser Irradiance

for free vibration of the plate.

(A-5) Over the time interval of interest, thermal diffusion in the radial direction is negligible. This condition can be expressed analytically as follows: $d^2/4Kt_p > 1$.

Note that assumptions (A-3) and (A-4) permit us to treat the plate as a semi-infinite solid when computing the temperature distribution. The temperature distribution induced in a semi-infinite solid by an incident, Gaussian laser pulse has been determined by J.H. Bechtel [3]. As a result of assumption (A-5), Bechtel shows that the temperature distribution is approximated by the function

$$T(r,z,t) = \frac{T_o}{\sqrt{\tau}} \exp[-(r/d)^2] \int_{-\infty}^{t} \exp[-(t'/\tau)^2] \cdot \exp[-z^2/4K(t-t')](t-t')^{-1/2} dt' \qquad (58)$$

where z is the distance measured into the solid from the irradiated surface and,

$$T_o = I_m(1-R)(\pi K_c \rho C)^{-1/2} \tau^{1/2} \qquad (59)$$

In (59), I_m is the maximum incident irradiance, R is the reflectivity of the plate surface, K_c, ρ, and C are the plate's thermal conductivity, density, and specific heat, respectively. Note that the thermal diffusivity $K=K_c/\rho C$.

A more convenient form of (58) is obtained by making the change of variable $\theta=(t-t')/\tau$. The result is,

$$T(r,z,t) = T_o \exp[-(r/d)^2] \int_{o}^{\infty} \exp[-(\frac{t}{\tau}-\theta)^2] \cdot \exp[-z^2/4K\tau\theta] \theta^{-1/2} d\theta \qquad (60)$$

4.2 Thermoelastic Forcing Functions

The thermoelastic forcing functions N_T and M_T are defined in (28) and rewritten here as follows:

$$N_T(r,t) = \alpha E \int_{-h/2}^{h/2} T dZ = \alpha E \int_{o}^{h} T dz \tag{61a}$$

$$M_T(r,t) = \alpha E \int_{-h/2}^{h/2} TZ dZ = \alpha E[\int_{o}^{h} Tz dz - \frac{h}{2}\int_{o}^{h} T dz] \tag{61b}$$

where $Z=z-h/2$ is measured from the middle surface of the plate as shown in Fig.1. Substitution of (60) into (61) yields the following results:

$$N_T(r,t) = N_o \exp[-(r/d)^2]N(t) \tag{62a}$$

$$M_T(r,t) = -M_o \exp[-(r/d)^2]M(t) \tag{62b}$$

where

$$\left.\begin{aligned} N_o &= \pi^{1/2}\alpha E I_m (1-R)\tau/\rho C \\ M_o &= N_o h/2 \end{aligned}\right\} \tag{63}$$

$$N(t) = \pi^{-1/2}\int_{o}^{\infty} \exp[-(\frac{t}{\tau}-\theta)^2]\operatorname{erf}(\phi)\,d\theta \tag{64a}$$

$$M(t) = \pi^{-1/2}\int_{o}^{\infty} \exp[-(\frac{t}{\tau}-\theta)^2]\{\operatorname{erf}(\phi) - 2\pi^{-1/2}[1-\exp(-\phi^2)]/\phi\}d\theta \tag{64b}$$

$$\phi = h(4K\tau\theta)^{-1/2} \tag{64c}$$

4.3 Numerical Values For Parameters

In order to compare the forthcoming analytical results for the motion of the plate with the experimental results, the following numerical values will be used for the parameters:

$E = 46.7 \times 10^{6}$ lb/in^2

$\nu = 0.33$

$\kappa^2 = 0.86$

$\rho = .7287606 \times 10^{-3}$ lb·sec^2/in^4

$K = .726 \times 10^{-2}$ in^2/sec.

$h = .0195$ in.

$a = 4.523$ in.

$A = a/d = 16$

$\tau = 40 \times 10^{-9}$ sec.

These parameters correspond to the experimental phase of this project, as described in Section 7 of this report.

5.0 FREE VIBRATION OF CLAMPED CIRCULAR PLATES.

5.1 Transverse Vibrations

In the case of axisymmetric, free, transverse vibrations,

$$w^{(i)}=w^{(i)}(R), \qquad \psi_r^{(i)}=\psi^{(i)}(R), \qquad \psi_\theta^{(i)}\equiv 0 \tag{65}$$

where R=r/a is a dimensionless radial coordinate. The stress-displacement relations become (see (55b)):

$$\left.\begin{aligned} M_{rr}^{(i)} &= \frac{D}{a}\left(\frac{d\psi^{(i)}}{dR}+\frac{\nu}{R}\psi^{(i)}\right) \\ M_{\theta\theta}^{(i)} &= \frac{D}{a}\left(\nu\frac{d\psi^{(i)}}{dR}+\frac{1}{R}\psi^{(i)}\right) \\ Q_r^{(i)} &= \kappa^2 Gh\left(\psi^{(i)}+\frac{1}{a}\frac{dw^{(i)}}{dR}\right) \end{aligned}\right\} \tag{66}$$

Substitution of (66) into (55a) yields the following homogeneous system of equations for the determination of the eigenfunctions: For $0\le R<1$,

$$\frac{d^2w^{(i)}}{dR^2}+\frac{1}{R}\frac{dw^{(i)}}{dR}+\ell\Omega_i^2 w^{(i)}+\frac{a}{R}\frac{d}{dR}\left(R\psi^{(i)}\right)=0 \tag{67a}$$

$$\frac{d^2\psi^{(i)}}{dR^2}+\frac{1}{R}\frac{d\psi^{(i)}}{dR}+\left(\Omega_i^2-\frac{1}{R^2}\right)\psi^{(i)}-\frac{1}{\ell H^2}\left(\psi^{(i)}+\frac{1}{a}\frac{dw^{(i)}}{dR}\right)=0 \tag{67b}$$

while at R=1,

$$w^{(i)}(1)=\psi^{(i)}(1)=0 \tag{67c}$$

In addition we require $w^{(i)}(0)$ and $\psi^{(i)}(0)$ to remain bounded. In (67),

$$\ell=\frac{E}{\kappa^2 G(1-\nu^2)}=\frac{2}{\kappa^2(1-\nu)} \tag{68a}$$

$$H^2=\frac{1}{12}\left(\frac{h}{a}\right)^2 \tag{68b}$$

$$\Omega_i^2 = \left(\frac{a}{v_p}\omega_i\right)^2 \tag{68c}$$

$$v_p^2 = \frac{E}{\rho(1-\nu^2)} \tag{68d}$$

The normalization condition (50) becomes:

$$2\pi a^2 \rho h \int_0^1 [(w^{(i)})^2 + H^2 a^2 (\psi^{(i)})^2] R dR = 1 \tag{69}$$

The solution of (67) through (69) is given in [1] (pp. 483-488). The following is a summary of that solution in a form amenable to numerical computations.

When solving equations (67), one naturally obtains a division of the frequency spectrum into two intervals, the low frequency range ($0<\ell H^2\Omega^2<1$), and the high frequency range ($\ell H^2\Omega^2>1$). The number of natural frequencies contained in the low frequency range increases as the thickness of the plate decreases. In fact, in the forthcoming forced motion example we will find that all the natural frequencies which contribute significantly to the solution are contained in the low frequency range. Therefore, the forthcoming analysis will be restricted to the low frequency range

$$0 < \ell H^2\Omega^2 < 1 \tag{70}$$

The frequency equation as well as the eigenfunctions can be expressed conveniently in terms of the parameter X which is related to the frequency Ω as follows: Let,

$$\lambda = H^2 X^2 \tag{71a}$$

$$\zeta = 1 + (\ell+1)\lambda \tag{71b}$$

and,

$$\mu = 2\ell\lambda^2/\zeta^2 \tag{71c}$$

Then,

$$\ell H^2\Omega^2 = \frac{1}{2}\,\zeta(1-\sqrt{1-2\mu}\,) \tag{71d}$$

In the low frequency range, $\mu<<1$ and therefore it is advisable to use a truncated Taylor series to compute the values of $\sqrt{1-2\mu}$. Substitution of this series into (71d) yields the alternate formula

$$H^2\Omega^2 = \lambda^2\eta \tag{72a}$$

where,

$$\eta = \xi/\zeta \tag{72b}$$

and,

$$\xi \cong 1+\mu(.5+\mu(.5+\mu(.625+\mu(.875 + \mu(1.3125 + \mu(2.0625)))))) \tag{72c}$$

In (72c), a sufficient number of terms have been retained in the Taylor series to yield values of ξ correct to at least eight significant figures. In view of (72a) and (71a) we conclude that

$$\Omega = \frac{\lambda}{H}\sqrt{\eta} = HX^2\sqrt{\eta} \tag{73}$$

This last equation is very revealing. For the lowest frequencies of a thin plate, $\lambda<<1$, therefore $\eta\cong 1$ and $\Omega\cong HX^2$.

In terms of the parameter X, the frequency equation may be written as follows:

$$J_o(X)I_1(Y) + f(X,Y)J_1(X)I_o(Y) = 0 \tag{74}$$

In (74), Y is related to X as follows:

Let,

$$\varepsilon = \frac{\ell\lambda}{\ell+1} \tag{75a}$$

$$p = 1 + \varepsilon\left(\frac{\ell^2+1}{\ell}\right) \tag{75b}$$

and,

$$\delta = -2\varepsilon(1-\varepsilon)/p^2 \tag{75c}$$

Then,

$$\varepsilon\left(\frac{Y}{X}\right)^2 = \frac{1}{2}p\left(\sqrt{1-2\delta} - 1\right) \tag{75d}$$

Since $\delta << 1$ in the low frequency range, $\sqrt{1-2\delta}$ may be computed from a truncated Taylor series, in which case (75d) is replaced by the following formula:

$$\left(\frac{Y}{X}\right)^2 = r = (1-\varepsilon)q/p \tag{76a}$$

where,

$$q \tilde{=} 1+\delta(.5+\delta(.5+\delta(.625+\delta(.875+\delta(1.3125+\delta(2.0625)))))) \tag{76b}$$

Consequently,

$$Y=sX \qquad \text{where } s = \sqrt{r} \tag{77}$$

Note that for the lowest frequencies of a thin plate, $s\tilde{=}1$ and therefore $Y\tilde{=}X$. The function $f(X,Y)$ appearing in (74) is defined as follows:

$$f(X,Y) = s/b \tag{78a}$$

where

$$b = (r+\ell)/(1+r\ell) \tag{78b}$$

Note that $f(X,Y)\tilde{=}1$ for the lowest frequencies of a thin plate. Combining this with the observation that $Y\tilde{=}X$, the lowest frequencies of a thin plate may be approximated by the roots of the equation

$$J_o(X)I_1(X) + J_1(X)I_o(X) = 0$$

which is in fact the frequency equation of classical plate theory for a clamped circular plate.

We note that the functions e^Y, $I_o(Y)$, and $I_1(Y)$ all increase

exponentially for large values of Y and have no positive real roots. Therefore, the frequency equation (74) can be modified by dividing the entire equation by $e^{-Y}I_o(Y)I_1(Y)$ without affecting its roots. This yields the modified frequency equation

$$F(X) = \frac{J_o(X)}{e^{-Y}I_o(Y)} + f(X,Y)\,\frac{J_1(X)}{e^{-Y}I_1(Y)} = 0 \qquad (79)$$

Equation (79) is more convenient to use in numerical computation than (74) since the maximum amplitudes of the oscillations in F(X) remain bounded as X increases. Furthermore, an examination of the asymptotic behavior of Bessel's functions reveals that the roots of (79) are approximately given by

$$\left.\begin{aligned} X_i &\cong i\pi \qquad \text{for } i=1,\ 2,\ 3,\ \ldots \\ X_i &\cong (i-\tfrac{1}{4})\pi \qquad \text{for } i=N,\ N-1,\ N-2,\ \ldots \end{aligned}\right\} \qquad (80)$$

where N represents the total number of frequencies in the low frequency range. The value of N is easily computed by noting that $\ell H^2\Omega^2<1$ implies that $\varepsilon<1$ which in turn implies that $X < \frac{1}{H}\sqrt{(\ell+1)/\ell}$. Therefore, N is the largest integer which is less than $(\frac{1}{4} + \frac{1}{\pi H}\sqrt{(\ell+1)/\ell}$. Using the parameters given in 4.3 yields N=290 in the present example. The first 35 roots of (79) were computed using a modified Newton-Raphson iteration technique with starting values of $X_1,\ldots X_{35}$ given by the first equation of (80). The modification was to use the first central difference [F(x+.0001)-F(x-.0001]/.0002 to approximate the derivative $\frac{dF}{dX}$ in the iteration formula. This technique yielded the roots to at least eight significant figures accuracy within two or three iterations. The first 35 values of X_i, Ω_i, and $\frac{\omega_i}{2\pi}$ are listed in Table I.

TABLE I

NATURAL FREQUENCIES OF TRANSVERSE VIBRATION

i	x_i	Y_i	Ω_i	$\frac{\omega_i}{2\pi}$
1	3.1961936E0	3.1960805E0	1.2713590E-2	1.1996775E2
2	6.3063102E0	6.3054420E0	4.9488953E-2	4.6698678E2
3	9.4392009E0	9.4362900E0	1.1085465E-1	1.0460447E3
4	1.2576589E1	1.2569707E1	1.9674580E-1	1.8565292E3
5	1.5715582E1	1.5702159E1	3.0711948E-1	2.8980354E3
6	1.8855303E1	1.8832134E1	4.4192713E-1	4.1701049E3
7	2.1995395E1	2.1958639E1	6.0111146E-1	5.6721973E3
8	2.5135686E1	2.5080875E1	7.8460586E-1	7.4036839E3
9	2.8276083E1	2.8198123E1	9.9233432E-1	9.3638475E3
10	3.1416533E1	3.1309709E1	1.2242114E0	1.1551882E4
11	3.4557000E1	3.4414983E1	1.4801426E0	1.3966895E4
12	3.7697463E1	3.7513317E1	1.7600241E0	1.6607908E4
13	4.0837906E1	4.0604093E1	2.0637432E0	1.9473857E4
14	4.3978319E1	4.3686708E1	2.3911786E0	2.2563598E4
15	4.7118694E1	4.6760569E1	2.7422005E0	2.5875904E4
16	5.0259026E1	4.9825092E1	3.1166707E0	2.9409473E4
17	5.3399310E1	5.2879706E1	3.5144430E0	3.3162924E4
18	5.6539543E1	5.5923849E1	3.9353633E0	3.7134805E4
19	5.9679724E1	5.8956969E1	4.3792702E0	4.1323592E4
20	6.2819849E1	6.1978525E1	4.8459949E0	4.5727691E4
21	6.5959920E1	6.4987989E1	5.3353615E0	5.0345443E4
22	6.9099933E1	6.7984840E1	5.8471876E0	5.5175128E4
23	7.2239889E1	7.0968572E1	6.3812842E0	6.0214961E4
24	7.5379788E1	7.3938691E1	6.9374563E0	6.5463102E4
25	7.8519629E1	7.6894711E1	7.5155031E0	7.0917657E4
26	8.1659411E1	7.9836162E1	8.1152181E0	7.6576677E4
27	8.4799136E1	8.2762584E1	8.7363897E0	8.2438165E4
28	8.7938803E1	8.5673531E1	9.3788013E0	8.8500079E4
29	9.1078413E1	8.8568568E1	1.0042232E1	9.4760331E4
30	9.4217966E1	9.1447274E1	1.0726456E1	1.0121679E5
31	9.7357462E1	9.4309240E1	1.1431244E1	1.0786730E5
32	1.0049690E2	9.7154069E1	1.2156363E1	1.1470966E5
33	1.0363629E2	9.9981378E1	1.2901576E1	1.2174162E5
34	1.0677562E2	1.0279080E2	1.3666644E1	1.2896094E5
35	1.0991489E2	1.0558197E2	1.4451324E1	1.3636533E5

The corresponding normalized eigenfunctions are given by the following:

For $0 \le R \le 1$,

$$w^{(i)} = \chi_i F_i^{(1)}(R) \tag{81a}$$

$$\psi^{(i)} = \chi_i \frac{X_i}{a} F_i^{(2)}(R) \tag{81b}$$

$$M_{rr}^{(i)} = \left(\frac{E}{1-\nu^2}\right) hH^2 \chi_i \left[X_i^2 F_i^{(4)}(R) - (1-\nu) X_i F_i^{(2)}(R)/R\right] \tag{81c}$$

$$M_{\theta\theta}^{(i)} = \left(\frac{E}{1-\nu^2}\right) hH^2 \chi_i \left[\nu X_i^2 F_i^{(4)}(R) + (1-\nu) X_i F_i^{(2)}(R)/R\right] \tag{81d}$$

$$Q_r^{(i)} = -\left(\frac{E}{1-\nu^2}\right) \frac{h}{a} \chi_i \frac{\Omega_i^2}{X_i} F_i^{(3)}(R) \tag{81e}$$

where,

$$F_i^{(1)} = J_o(X_i R) - c_i I_o(Y_i R) \tag{82a}$$

$$F_i^{(2)} = a_i \left[J_1(X_i R) - d_i I_1(Y_i R)\right] \tag{82b}$$

$$F_i^{(3)} = J_1(X_i R) + \frac{d_i}{b_i} I_1(Y_i R) \tag{82c}$$

$$F_i^{(4)} = a_i \left[J_o(X_i R) + b_i c_i I_o(Y_i R)\right] \tag{82d}$$

and,

$$\chi_i^2 = \frac{1}{2\pi a^2 \rho h P_i^2} \tag{83a}$$

$$P_i^2 = A_i J_o^2(X_i) + B_i J_1^2(X_i) - C_i J_o(X_i) J_1(X_i) \tag{83b}$$

$$A_i = 1 - \frac{1}{2} \lambda_i a_i^2 \left(\frac{b_i^2}{r_i} - 1\right) \tag{83c}$$

$$B_i = \frac{1}{2}(1-f_i^2) + \lambda_i a_i^2 \tag{83d}$$

$$C_i = \frac{2(1-r_i f_i)}{X_i(1+r_i)} \left[1 + (1+\ell) a_i^2 b_i \eta_i \lambda_i^2/(2r_i)\right] \tag{83e}$$

$$
\left.
\begin{aligned}
a_i &= (1+r_i\ell)/(1+\ell) \\
b_i &= (r_i+\ell)/(1+r_i\ell) \\
c_i &= J_o(X_i)/I_o(Y_i) \\
d_i &= J_1(X_i)/I_1(Y_i) \\
\beta_i &= s_i d_i \\
\alpha_i^o &= [\frac{\pi}{2} x_i \eta_i p_i^2]^{-1} \\
e_i &= a_i \alpha_i^o / X_i \\
f_i &= f(X_i, Y_i)
\end{aligned}
\right\} \qquad (84)
$$

5.2 Extensional Vibrations

In the case of axisymmetric, free, extensional vibrations,

$$u_r^{(i)} = u^{(i)}(R), \qquad u_\theta^{(i)} \equiv 0 \qquad (85)$$

$$N_{rr}^{(i)} = \frac{Eh}{a(1-\nu^2)} \left(\frac{du^{(i)}}{dR} + \frac{\nu}{R} u^{(i)}\right) \qquad (86a)$$

$$N_{\theta\theta}^{(i)} = \frac{Eh}{a(1-\nu^2)} \left(\nu \frac{du^{(i)}}{dR} + \frac{1}{R} u^{(i)}\right) \qquad (86b)$$

Substitution of (86) into (52b) yields the following homogeneous system of equations for the determination of the eigenfunctions:

For $0 \le R < 1$,

$$\frac{d^2u^{(i)}}{dR^2} + \frac{1}{R}\frac{du^{(i)}}{dR} + \left(\Omega_i^2 - \frac{1}{R^2}\right)u^{(i)} = 0 \qquad (87a)$$

while at $R=1$,

$$u^{(i)}(1) = 0 \qquad (87b)$$

We also require $u^{(i)}(0)$ to remain bounded. The corresponding normalization condition (44d) becomes,

$$2\pi a^2 \rho h \int_0^1 (u^{(i)})^2 R dR = 1 \tag{88}$$

The solution of (87) and (88) can easily be shown to be

$$u^{(i)}(R) = A_i J_1(\Omega_i R) \tag{89a}$$

$$N_{rr}^{(i)}(R) = \frac{EhA_i}{a(1-\nu^2)} \left[\Omega_i J_o(\Omega_i R) - \frac{(1-\nu)}{R} J_1(\Omega_i R)\right] \tag{89b}$$

$$N_{\theta\theta}^{(i)}(R) = \frac{EhA_i}{a(1-\nu^2)} \left[\nu\Omega_i J_o(\Omega_i R) + \frac{(1-\nu)}{R} J_1(\Omega_i R)\right] \tag{89c}$$

where,

$$\frac{1}{A_i^2} = \pi a^2 \rho h J_o^2(\Omega_i) \tag{89d}$$

and,

$$J_1(\Omega_i) = 0, \qquad i=1,2,3,\ldots \ . \tag{90}$$

An examination of the asymptotic form of $J_1(\Omega)$ reveals that the natural frequencies are approximately given by

$$\Omega_i \cong (i + \tfrac{1}{4})\pi \ , \qquad i=1,2,3,\ldots \ .$$

Table II lists the first 30 natural frequencies taken from [4] (p. 748 Table VII). The corresponding values of $J_o(\Omega_i)$ and $\alpha_i^o = [\frac{\pi}{2}\Omega_i J_o^2(\Omega_i)]^{-1}$ are also listed for convenience in future computations.

TABLE II

NATURAL FREQUENCIES OF EXTENSIONAL VIBRATION

i	Ω_i	$J_o(\Omega_i)$	α_i^o
1	3.8317060	-.4027593957	1.024227855
2	7.0155867	.3001157525	1.007484896
3	10.1734681	-.2497048771	1.003591665
4	13.3236919	.2183594072	1.002101537
5	16.4706301	-.1964653715	1.001377622
6	19.6158585	.1800633753	1.000972230
7	22.7600844	-.1671846005	1.000722608
8	25.9036721	.1567249863	1.000558091
9	29.0468285	-.1480111100	1.000443971
10	32.1896799	.1406057982	1.000361582
11	35.3323076	-.1342112403	1.000300165
12	38.4747662	.1286166221	1.000253167
13	41.6170942	-.1236679608	1.000216398
14	44.7593190	.1192498120	1.000187095
15	47.9014609	-.1152736941	1.000163364
16	51.0435352	.1116704969	1.000143877
17	54.1855536	-.1083853489	1.000127682
18	57.3275254	.1053740554	1.000114073
19	60.4694578	-.1026005671	1.000102530
20	63.6113567	.1000351468	1.000092653
21	66.7532267	-.0976530158	1.000084139
22	69.8950718	.0954333390	1.000076746
23	73.0368952	-.0933584533	1.000070287
24	76.1786996	.0914132722	1.000064609
25	79.3204872	-.0895848220	1.000059593
26	82.4622599	.0878618760	1.000055139
27	85.6040194	-.0862346634	1.000051167
28	88.7457671	.0846946348	1.000047609
29	91.8875043	-.0832342730	1.000044408
30	95.0292318	.0818469379	1.000041521

$$\alpha_i^o = \left[\frac{\pi}{2}\,\Omega_i J_o^2(\Omega_i)\right]^{-1}$$

6.0 FORCED MOTION OF THE CLAMPED CIRCULAR PLATE

6.1 Transverse Motion

In the subsequent forced motion analysis we shall find it convenient to introduce a dimensionless time scale based on the fundamental period of free transverse vibrations. Thus, we define

$$t_1 = \frac{\omega_1}{2\pi} t = (119.96775)t \tag{91a}$$

or, conversely,

$$t = \frac{2\pi}{\omega_1} t_1 = (8.3355736 \times 10^{-3})t_1 \tag{91b}$$

The thermoelastic bending moment M_T is given by (62b) with M(t) defined in (64). A very accurate closed form approximation of M(t) can be obtained from (64b) as follows. The term $\exp[-(\frac{t}{\tau} - \theta)^2]$ tends to strongly focus our attention on those values of θ for which $|\frac{t}{\tau} - \theta| < 5$. Indeed, when $|\frac{t}{\tau} - \theta| \geq 5$ then $\exp[-(\frac{t}{\tau} - \theta)^2] \leq 1.4 \times 10^{-11}$ and the contributions to the integral in this range are negligible. The smallest time of interest in the forced motion solution is on the order of $\frac{1}{100}$ of the fundamental period. Thus, the time interval of interest corresponds to $t_1 \geq .01$ or $t \geq 8.336 \times 10^{-5}$ or $\frac{t}{\tau} \geq 2084$. At $\frac{t}{\tau} = 2084$, the inequality $|\frac{t}{\tau} - \theta| < 5$ yields the inequality $2079 < \theta < 2089$ which when substituted into (64c) yields the result $12.52 < \phi < 12.54$. Note that ϕ is essentially constant over the range of values of θ required to evaluate the integral (64b) for this instant of time. Furthermore, if $\frac{t}{\tau} > 2084$ then ϕ varies even less over the range of values of θ needed to perform the integration. Consequently, for $t_1 \geq .01$, ϕ can be considered a constant in the integral (64b) with $\theta = \frac{t}{\tau}$, i.e.,

$$\phi = h(4Kt)^{-1/2} = h\left(\frac{\omega_1}{8\pi K t_1}\right)^{1/2} \tag{92a}$$

or

$$\phi = 1.2533390\ t_1^{-1/2} \tag{92b}$$

After removing the constant expression involving ϕ from the integral, all that remains to be integrated is

$$\pi^{-1/2} \int_0^\infty \exp[-(\frac{t}{\tau} - \theta)^2]d\theta = \frac{1}{2}[1+\text{erf}(\frac{t}{\tau})] = 1$$

since $\frac{t}{\tau} \geq 2084$ and erf(x) is one to ten decimal places for any x>5. We thus arrive at the following approximation for the thermoelastic bending moment:

$$M(t_1) = \text{erf}(\phi) - 2\pi^{-1/2}[1-\exp(-\phi^2)]/\phi \tag{93}$$

According to (64b), M(0)=1/2 but M(t) very quickly increases to 1. Since this rise time is less than $\frac{1}{100}$ of the fundamental period we will simply assume that M(0)=1 as predicted by (93). As a result of these observations we shall henceforth use (62b) with $M(t_1)$ given by (93) to represent the thermoelastic bending moment. A graph of $M(t_1)$ vs. t_1 is shown in Fig. (2).

The generalized force $Q_i(t_1)$ is now evaluated by substituting (62b) into (57). The result is,

$$\begin{aligned}\omega_i^2 Q_i(t_1) &= (\frac{2\pi a}{1-\nu})M_o M(t_1) \int_0^1 e^{-A^2R^2} \frac{d}{dR}(R\psi^{(i)})dR \\ &= (\frac{4\pi a}{1-\nu})A^2 M_o M(t_1) \int_0^1 R^2 e^{-A^2R^2}\psi^{(i)}\, dR\end{aligned} \tag{94}$$

where $A = \frac{a}{d}$ is the spot ratio. Consider the integral

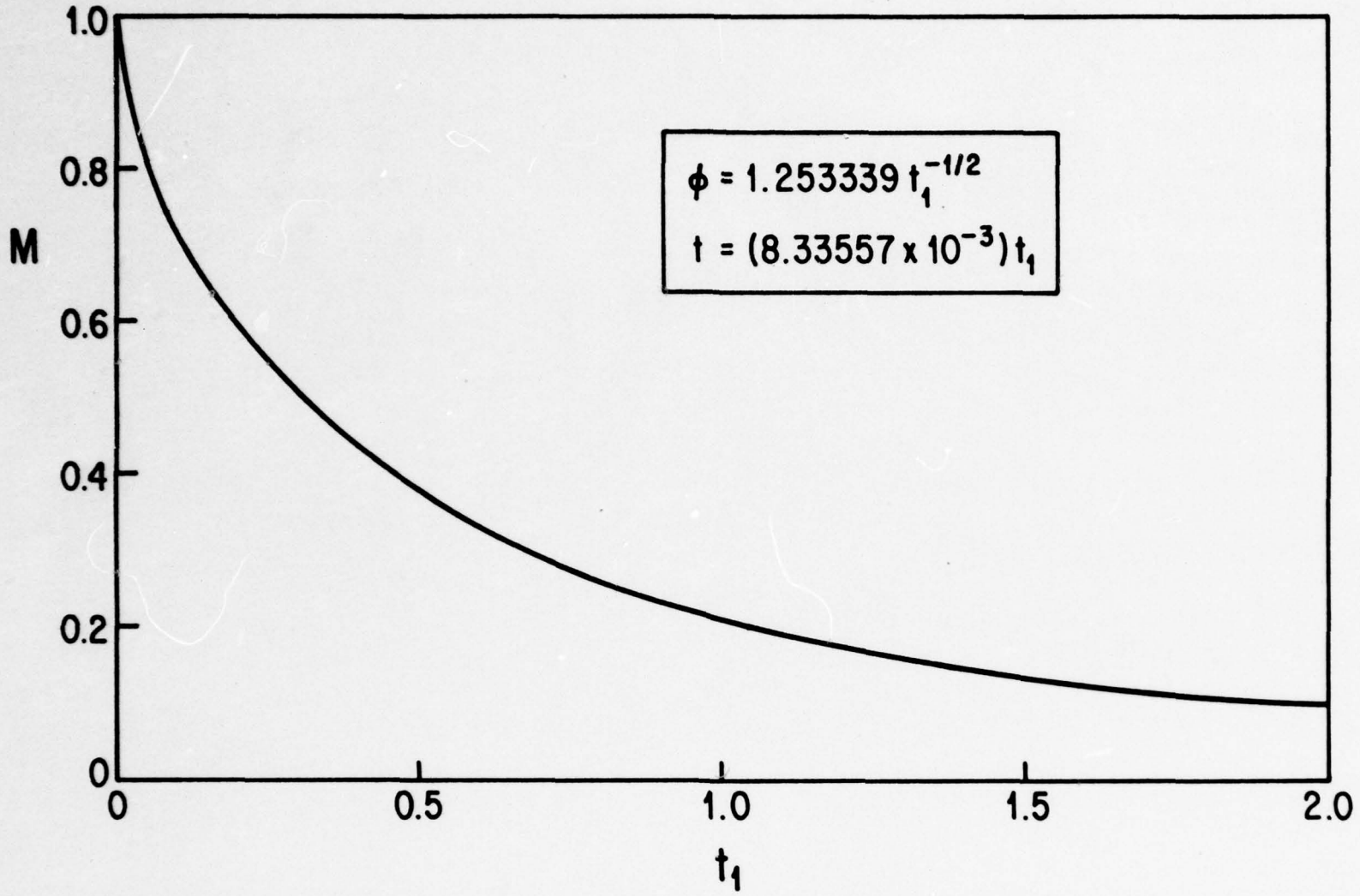

Figure 2: Thermal Bending Moment $M(t_1)$ vs. t_1.

$$I = \int_0^1 R^2 e^{-A^2R^2} \psi^{(i)} dR \tag{95}$$

By substituting (81b) and (82b) into (95) we obtain

$$I = \frac{1}{a} \chi_i X_i a_i \int_0^1 R^2 e^{-A^2R^2} [J_1(X_i R) - d_i I_1(Y_i R)] dR$$

Notice that at R=1, $e^{-A^2R^2} = e^{-256} = 6.6 \times 10^{-112}$ and therefore the upper limit of the integral can be extended to infinity without noticably affecting the value of I. This technique allows us to obtain the following closed form expression for I:

$$I = \frac{\chi_i X_i a_i}{4A^4 a} \{X_i \exp[-(X_i/2A)^2] - d_i Y_i \exp[(Y_i/2A)^2]\} \tag{96}$$

Substitution of (96) into (94) then yields the desired result,

$$\chi_i Q_i(t_1) = \frac{\pi M_o (1+\nu)}{4A^2 Eh} \frac{K_i}{H^2} M(t_1) \tag{97a}$$

where

$$K_i = e_i \{\exp[-(X_i/2A)^2] - \beta_i \exp[(Y_i/2A)^2]\} \tag{97b}$$

with e_i and β_i defined in (84). Further substitution of (97) into the second of (57) yields the result

$$\chi_i q_i(t_1) = \frac{\pi M_o (1+\nu)}{4A^2 Eh} \frac{K_i}{H^2} g_i(t_1) \tag{98a}$$

where,

$$g_i(t_1) = M(t_1) - 2\pi R_i \int_0^{t_1} M(\theta) \sin 2\pi R_i (t_1 - \theta) d\theta \tag{98b}$$

and where

$$R_i = \frac{\omega_i}{\omega_1}, \quad i=1,2,3,... \tag{98c}$$

An efficient scheme for the numerical evaluation of $g_i(t_1)$ is given

in Appendix I.

The quasi-static problem for the present example is characterized by the following equations:

For $0 \leq R < 1$,

$$\frac{1}{R}\frac{d}{dR}(RQ_r^{(s)}) = 0 \tag{99a}$$

$$\frac{dM_{rr}^{(s)}}{dR} + \frac{1}{R}(M_{rr}^{(s)} - M_{\theta\theta}^{(s)}) = aQ_r^{(s)} \tag{99b}$$

where,

$$Q_r^{(s)} = \frac{1}{a}\kappa^2 Gh(a\psi^{(s)} + \frac{dw^{(s)}}{dR}) \tag{100a}$$

$$M_{rr}^{(s)} = \frac{D}{a}(\frac{d\psi^{(s)}}{dR} + \frac{\nu}{R}\psi^{(s)}) - \frac{M_T}{1-\nu} \tag{100b}$$

$$M_{\theta\theta}^{(s)} = \frac{D}{a}(\nu\frac{d\psi^{(s)}}{dR} + \frac{1}{R}\psi^{(s)}) - \frac{M_T}{1-\nu} \tag{100c}$$

The corresponding boundary conditions are:

$$w^{(s)}(1) = \psi^{(s)}(1) = 0 \tag{101}$$

while, $w^{(s)}(0)$ and $\psi^{(s)}(0)$ remain bounded.

The solution of (99) through (101) is summarized below.

$$w^{(s)}(R,t_1) = -\frac{M_o a^2}{DA^2(1-\nu)} M(t_1)W_s(R) \tag{102a}$$

$$\psi^{(s)}(R,t_1) = -\frac{M_o a}{DA^2(1-\nu)} M(t_1)\Psi_s(R) \tag{102b}$$

$$M_{rr}^{(s)}(R,t_1) = \frac{M_o}{2} M(t_1)M_{RS}(R) \tag{102c}$$

$$M_{\theta\theta}^{(s)}(R,t_1) = \frac{M_o}{2} M(t_1)M_{\theta S}(R) \tag{102d}$$

$$Q_r^{(s)}(R,t_1) \equiv 0 \tag{102e}$$

where,

$$W_s(R) = -\frac{1}{4}[(1-R^2)(1-e^{-A^2}) + \ln R^2 + E_1(A^2R^2) - E_1(A^2)] \tag{103a}$$

$$\Psi_s(R) = \frac{1}{2}[\frac{1}{R}(1-e^{-A^2R^2}) - R(1-e^{-A^2})] \tag{103b}$$

$$M_{RS}(R) = \frac{1}{A^2R^2}(1-e^{-A^2R^2}) + \frac{1}{A^2}(\frac{1+\nu}{1-\nu})(1-e^{-A^2}) \tag{103c}$$

$$M_{\theta S}(R) = 2e^{-A^2R^2} - \frac{1}{A^2R^2}(1-e^{-A^2R^2}) + \frac{1}{A^2}(\frac{1+\nu}{1-\nu})(1-e^{-A^2}) \tag{103d}$$

In (103a), $E_1(X)$ is the exponential integral defined as follows:

$$E_1(X) = \int_x^\infty \frac{e^{-t}}{t}\,dt = \int_o^x (1-e^{-t})\,\frac{dt}{t} - \ln x - \gamma \tag{104}$$

where $\gamma = .5772156649\ldots$ is Euler's constant. In the limit as $R \to 0$, (103a) becomes

$$W_s(0) = \frac{1}{4}[\ln A^2 + E_1(A^2) + \gamma - (1-e^{-A^2})] \tag{105}$$

Fig. (3) shows the radial variation of the quasi-static deflection $W_s(R)$. As expected the maximum deflection occurs at the center of the plate. Fig. (4) shows the radial variation of the quasi-static bending moments. Again the maximum moment occurs at the center of the plate where $M_{RS} = M_{\theta S}$. The complete forced motion solution is now obtained by substituting (102), (98), and (81) into (48). The results are

$$w(R,t_1) = -\frac{M_o(1+\nu)}{A^2H^2Eh}[W_S(R)M(t_1) - S_1(R,t_1)] \tag{106a}$$

$$M_{rr}(R,t_1) = \frac{M_o}{2}[M_{RS}(R)M(t_1) + S_2(R,t_1)] \tag{106b}$$

$$M_{\theta\theta}(R,t_1) = \frac{M_o}{2}[M_{\theta S}(R)M(t_1) + S_3(R,t_1)] \tag{106c}$$

$$Q_r(R,t_1) = -\frac{M_o}{2d(1-\nu)}\,S_4(R,t_1) \tag{106d}$$

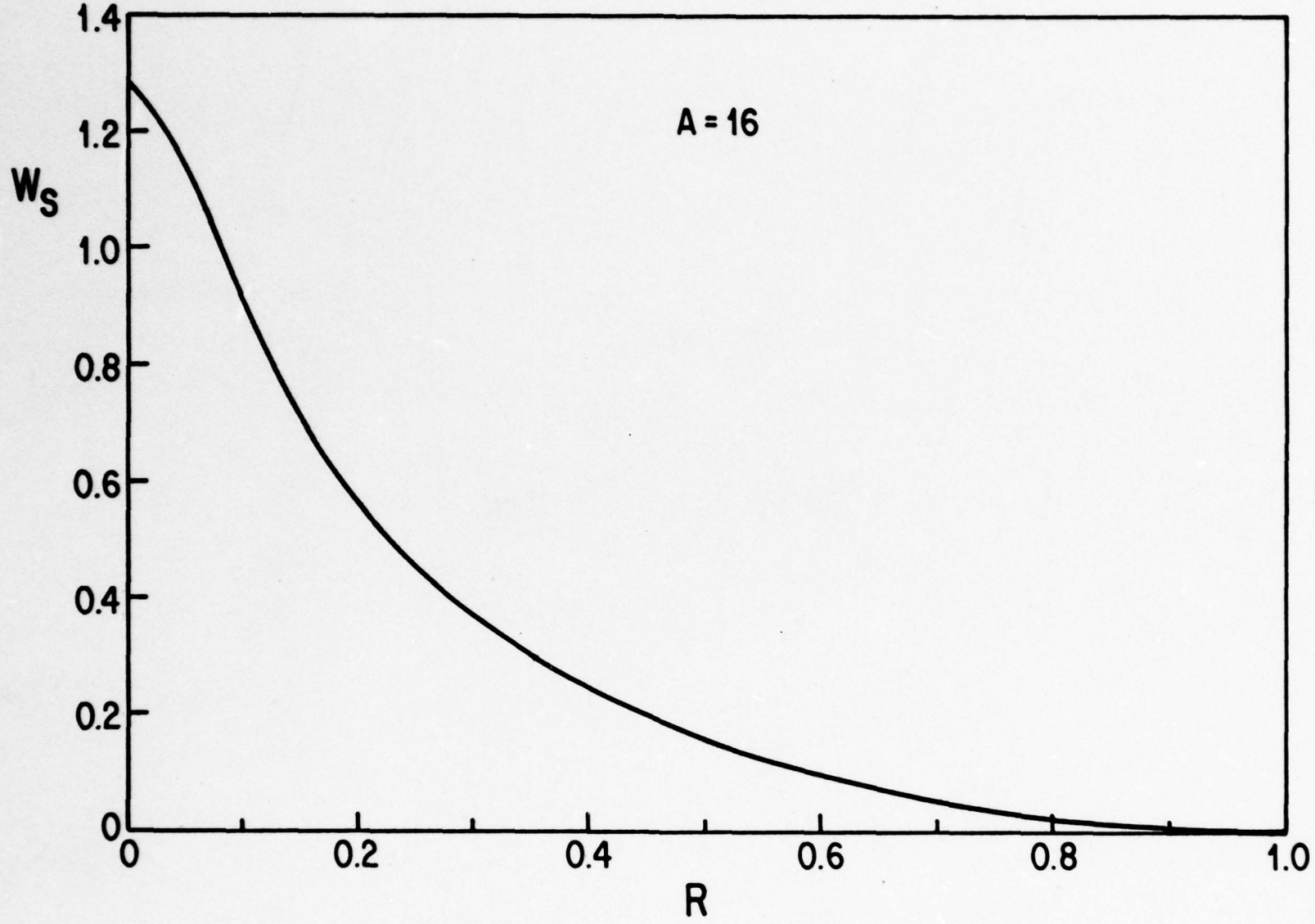

Figure 3: Quasi-Static Deflection $W_S(R)$ vs. R

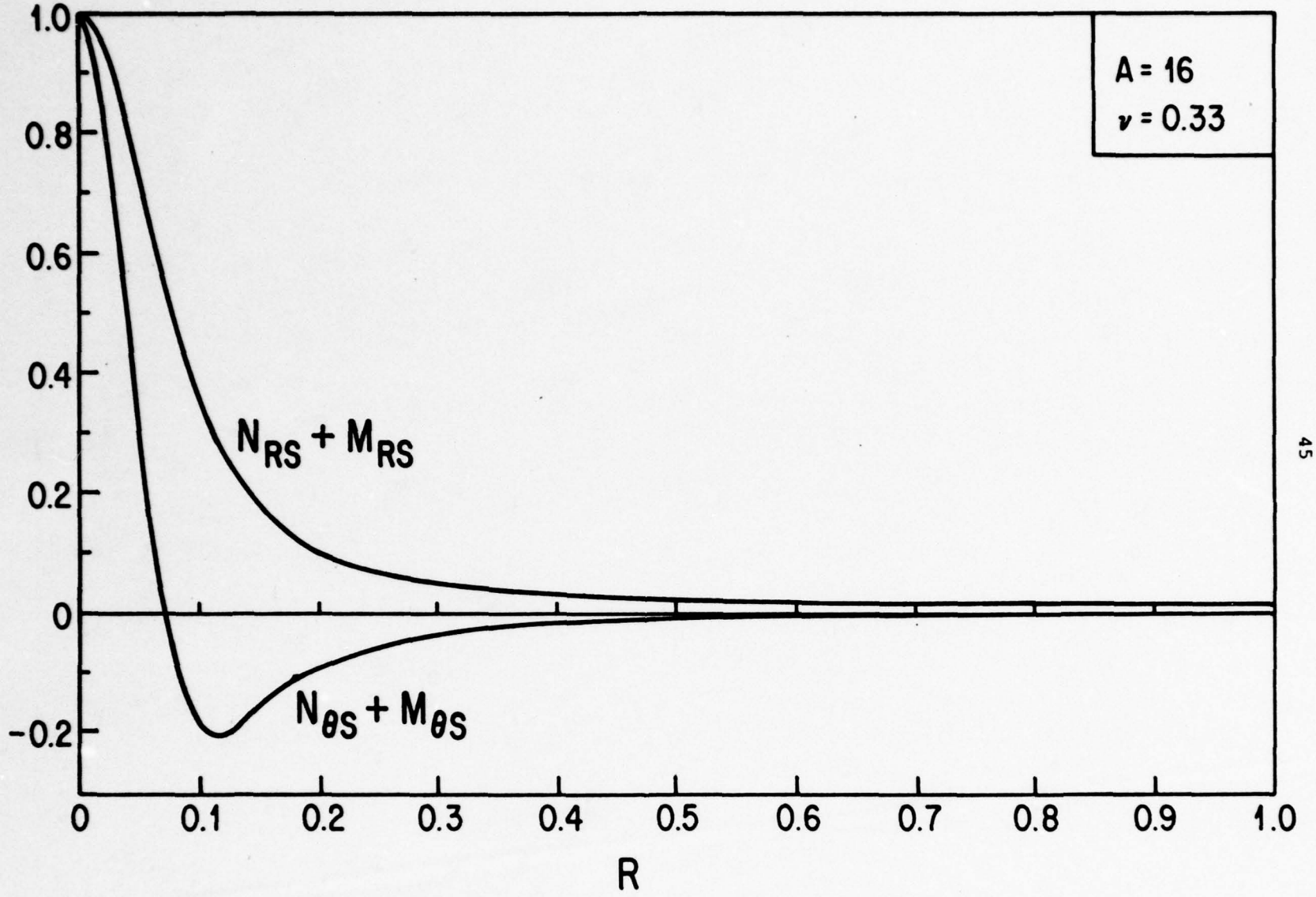

Figure 4: Quasi-Static Bending Moments and Normal Forces
$M_{RS} = N_{RS}$ and $M_{\theta S} = N_{\theta S}$

where,

$$S_1(R,t_1) = \frac{\pi}{4} \sum_{i=1}^{\infty} K_i F_i^{(1)}(R) g_i(t_1) \tag{107a}$$

$$S_2(R,t_1) = \frac{\pi}{2A^2} \sum_{i=1}^{\infty} K_i X_i^2 \left[\frac{F_i^{(4)}(R)}{1-\nu} - \frac{F_i^{(2)}(R)}{X_i R}\right] g_i(t_1) \tag{107b}$$

$$S_3(R,t_1) = \frac{\pi}{2A^2} \sum_{i=1}^{\infty} K_i X_i^2 \left[\frac{\nu F_i^{(4)}(R)}{1-\nu} + \frac{F_i^{(2)}(R)}{X_i R}\right] g_i(t_1) \tag{107c}$$

$$S_4(R,t_1) = \frac{\pi}{2A^3} \sum_{i=1}^{\infty} K_i \frac{\Omega_i^2}{H^2 X_i} F_i^{(3)}(R) g_i(t_1) \tag{107d}$$

Since the maximum deflection and moment occurs at the center of the plate, we set R=0 in (107) to obtain:

$$S_1(0,t_1) = \sum_{i=1}^{\infty} S_1^{(i)} g_i(t_1) \tag{108a}$$

$$S_2(0,t_1) = \sum_{i=1}^{\infty} S_2^{(i)} g_i(t_1) \tag{108b}$$

$$S_3(0,t_1) = \sum_{i=1}^{\infty} S_3^{(i)} g_i(t_1) = S_2(0,t) \tag{108c}$$

where,

$$S_1^{(i)} = \frac{\pi}{4} K_i D_1^{(i)} \tag{108d}$$

$$S_2^{(i)} = \frac{\pi}{2} K_i \frac{X_i^2}{A^2} \left(\frac{D_2^{(i)}}{1-\nu} - D_3^{(i)}\right) \tag{108e}$$

$$S_3^{(i)} = \frac{\pi}{2} K_i \frac{X_i^2}{A^2} \left(\frac{\nu D_2^{(i)}}{1-\nu} + D_3^{(i)}\right) = S_2^{(i)} \tag{108f}$$

and,

$$D_1^{(i)} = 1-c_i \tag{108g}$$

$$D_2^{(i)} = a_i(1+b_ic_i) \tag{108h}$$

$$D_3^{(i)} = \frac{1}{2}a_i(1-\beta_i) \tag{108i}$$

The first 35 values of $S_1^{(i)}$, $S_2^{(i)}$, and K_i are presented in Table III. This table shows that by summing the first 35 values we are guaranteed at least 4 significant figures of accuracy in our final results. Fig. (5) is a graph of the dimensionless, negative displacement at the center of the plate:

$$W(0,t_1) = W_S(0)M(t_1) - S_1(0,t_1) \tag{109}$$

The negative displacement was used to facilitate later comparison with the experimental results. The periodic nature of $S_1(0,t_1)$ is evident in this graph with the second cycle beginning at approximately t_1=1.04. The large initial slope of the deflection curve indicates that the thermoelastic forcing of the plate behaves somewhat like an impulse (finite initial velocity-slope) or perhaps even a doublet (infinite initial velocity-slope). Fig. 6 shows the dimensionless bending moment at the center of the plate

$$\frac{M_{rr}(0,t_1)}{M_o} = \frac{M_{\theta\theta}(0,t_1)}{M_o} = \frac{1}{2}[M_{RS}(0)M(t_1) + S_2(0,t_1)] \tag{110}$$

The very nervous behavior of the bending moment reinforces the previous observation concerning the singular nature of the thermoelastic forcing of the plate.

TABLE III

MODAL CONSTANTS FOR TRANSVERSE MOTION

i	K_i	$S_1^{(i)}$	$S_2^{(i)}$
1	5.7112283E-1	4.7355160E-1	3.3550525E-2
2	3.0456808E-1	2.3860149E-1	7.3937955E-2
3	1.9384665E-1	1.5226375E-1	1.0512335E-1
4	1.3612248E-1	1.0690983E-1	1.3101330E-1
5	9.9915163E-2	7.8473202E-2	1.5008695E-1
6	7.4913310E-2	5.8836776E-2	1.6189144E-1
7	5.6661747E-2	4.4502032E-2	1.6651482E-1
8	4.2911681E-2	3.3702756E-2	1.6455553E-1
9	3.2382838E-2	2.5433422E-2	1.5700721E-1
10	2.4270102E-2	1.9061693E-2	1.4511752E-1
11	1.8022708E-2	1.4155002E-2	1.3024004E-1
12	1.3237398E-2	1.0396628E-2	1.1369863E-1
13	9.6038165E-3	7.5428198E-3	9.6678676E-2
14	6.8753734E-3	5.3999057E-3	8.0153195E-2
15	4.8529442E-3	3.8114935E-3	6.4845915E-2
16	3.3750873E-3	2.6507874E-3	5.1227596E-2
17	2.3115416E-3	1.8154805E-3	3.9538539E-2
18	1.5583386E-3	1.2239162E-3	2.9828264E-2
19	1.0337209E-3	8.1188251E-4	2.2003407E-2
20	6.7451118E-4	5.2975984E-4	1.5876155E-2
21	4.3281518E-4	3.3993225E-4	1.1207604E-2
22	2.7305041E-4	2.1445329E-4	7.7427371E-3
23	1.6932583E-4	1.3298820E-4	5.2357548E-3
24	1.0319717E-4	8.1050872E-5	3.4661286E-3
25	6.1803085E-5	4.8540029E-5	2.2467710E-3
26	3.6365677E-5	2.8561536E-5	1.4262052E-3
27	2.1021345E-5	1.6510126E-5	8.8668192E-4
28	1.1936320E-5	9.3747641E-6	5.3996324E-4
29	6.6570270E-6	5.2284168E-6	3.2211724E-4
30	3.6463055E-6	2.8638017E-6	1.8825904E-4
31	1.9613512E-6	1.5404416E-6	1.0780150E-4
32	1.0359937E-6	8.1366755E-7	6.0485680E-5
33	5.3731758E-7	4.2200824E-7	3.3255850E-5
34	2.7362285E-7	2.1490289E-7	1.7918336E-5
35	1.3680389E-7	1.0744552E-7	9.4616222E-6

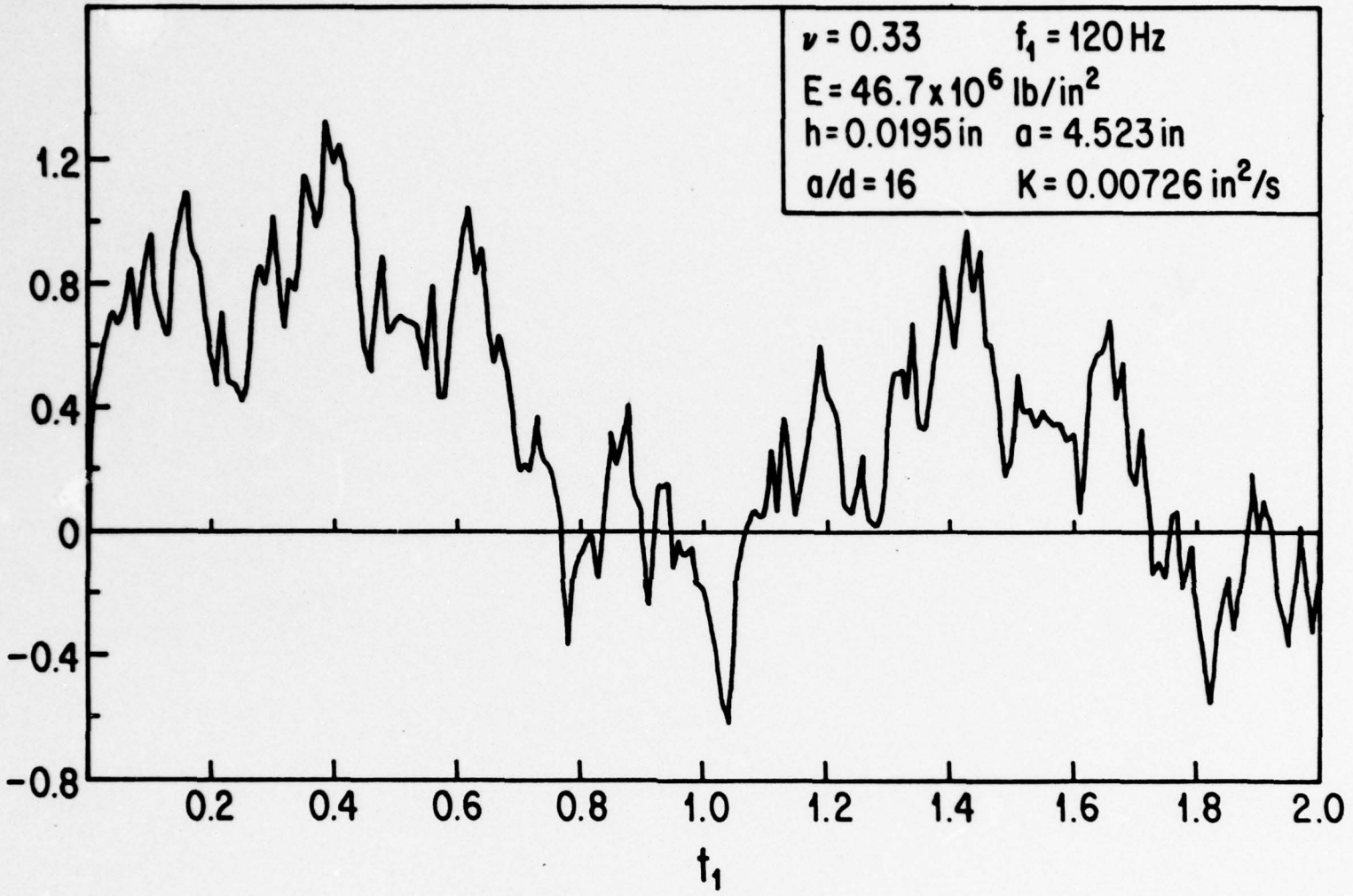

Figure 5: Displacement vs. Time

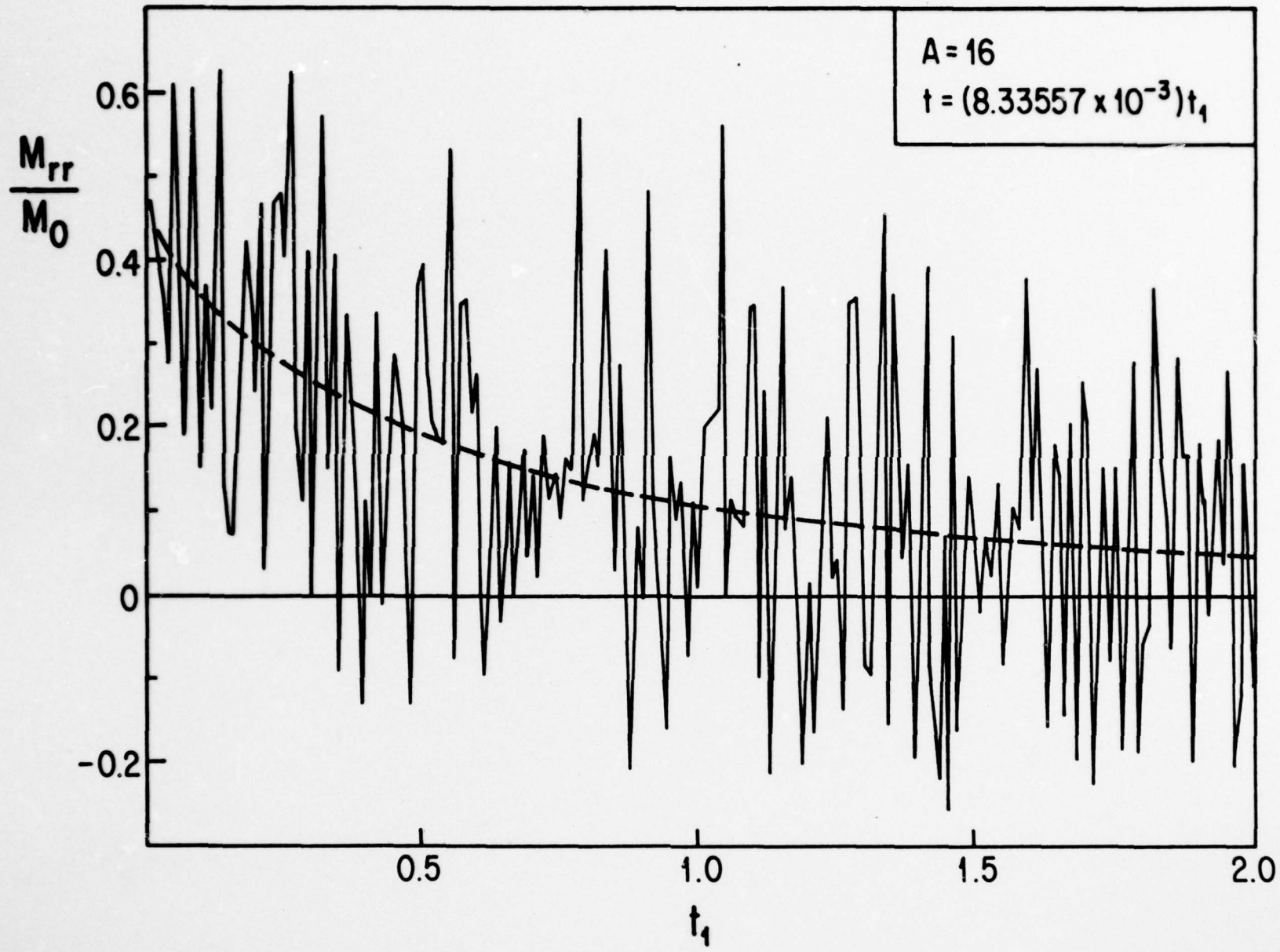

Figure 6: Bending Moment at R = 0 vs. Time

6.2 Extensional Motion

As in 6.1, we shall introduce a dimensionless time scale based on the fundamental period of free extensional vibrations, i.e.,

$$t_2 = \frac{\omega_1}{2\pi} t = (36156.676)t \tag{111a}$$

or conversely,

$$t = \frac{2\pi}{\omega_1} t_2 = (.027657410 \times 10^{-3})t_2 \tag{111b}$$

An accurate approximation of the thermoelastic normal force N_T can be obtained in a manner similar to that used in section 6.1. The reasoning goes as follows. The time interval of interest in the present problem corresponds to the first few cycles of the extensional motion. Thus, we shall consider the interval $.01 \le t_2 \le 10$ which implies $6.915 \le \frac{t}{\tau} \le 6915$. Since $|\theta - \frac{t}{\tau}| \le 5$, $1.915 \le \theta \le 6920$ and therefore $6.876 \le \phi \le 413$. In this interval, $\text{erf}(\phi)=1$ to more than ten decimal places and therefore (64a) becomes,

$$N(t) = \pi^{-1/2} \int_0^\infty \exp[-(\frac{t}{\tau} - \theta)^2]d\theta = \frac{1}{2}[1+\text{erf}(\frac{t}{\tau})] = 1$$

since $\text{erf}(\frac{t}{\tau})$ is also equal to one in the time interval of interest. Thus, we shall use $N(t)=1$ for $t>0$, or

$$N_T(R,t) = N_o \exp[-(r/d)^2] \text{ for } t>0 \tag{112}$$

The generalized force $Q_i(t_2)$ is now obtained by substituting (112) and (89a) into (54). The result is

$$\omega_i^2 Q_i(t_2) = -(\frac{N_o}{1-\nu})2\pi a^2 \frac{\Omega_i}{a} A_i \int_0^1 J_o(\Omega_i R) e^{-A^2R^2} RdR.$$

Again, noting that $e^{-A^2R^2} = 6.6 \times 10^{-112}$ at $R=1$, we may extend the upper

limit in the above integral to infinity without noticably affecting the value of the integral to obtain:

$$\int_0^1 J_o(\Omega_i R) e^{-A^2R^2} R dR \tilde{=} \frac{1}{2A^2} e^{-\Omega_i^2/4A^2}$$

Thus,

$$Q_i(t_2) = -\left(\frac{N_o}{1-\nu}\right) \frac{a\pi A_i d^2}{\Omega_i v_p^2} \exp\left[-\left(\frac{\Omega_i}{2A}\right)^2\right] \tag{113a}$$

and

$$q_i(t_2) = -\left(\frac{N_o}{1-\nu}\right) \frac{a\pi A_i d^2}{\Omega_i v_p^2} \exp\left[-\left(\frac{\Omega_i}{2A}\right)^2\right] \cos 2\pi R_i t_2 \tag{113b}$$

where, $R_i = \frac{\omega_i}{\omega_1}$, $i=1,2,3,\ldots$.

The corresponding quasi-static problem is characterized by the equation

$$\frac{d}{dR}\left[\frac{1}{R}\frac{d}{dR}\left(Ru^{(s)}\right)\right] = a\left(\frac{1+\nu}{Eh}\right)\frac{dN_T}{dR}, \qquad 0 \le R < 1 \tag{114}$$

where $u^{(s)}(1)=0$ and $u^{(s)}(0)$ is bounded. The solution of (114) is readily found to be

$$\frac{u^{(s)}}{d} = \frac{N_o(1+\nu)}{2Eh} U_s(R) \tag{115a}$$

where,

$$U_s(R) = AR\left[\frac{1}{A^2R^2}\left(1-e^{-A^2R^2}\right) - \frac{1}{A^2}\left(1-e^{-A^2}\right)\right] \tag{115b}$$

Substitution of (115) into (52c) yields the normal forces

$$\frac{N_{rr}^{(s)}}{N_o} = -\frac{1}{2} N_{RS}(R) \tag{116a}$$

$$\frac{N_{\theta\theta}^{(s)}}{N_o} = -\frac{1}{2} N_{\theta S}(R) \tag{116b}$$

where $N_{RS}(R)=M_{RS}(R)$ and $N_{\theta S}(R)=M_{\theta S}(R)$, (see eq. (103)). The radial variation of the dimensionless displacement $U_S(R)$ is shown in Fig. (7). Note that the maximum displacement occurs approximately at R=0.07 and thus that is where we shall study the motion of the plate.

The total solution is now obtained by substituting (115), (116), (113), and (89) into (53). The result is:

$$\frac{u(R,t_2)}{d} = \frac{N_o(1+\nu)}{2Eh} [U_s(R)-S_1(R,t_2)] \tag{117a}$$

$$\frac{N_{rr}(R,t_2)}{N_o} = -\frac{1}{2}[N_{RS}(R) - \frac{S_1(R,t_2)}{AR} + \frac{S_o(R,t_2)}{1-\nu}] \tag{117b}$$

$$\frac{N_{\theta\theta}(R,t_2)}{N_o} = -\frac{1}{2}[N_{\theta S}(R) + \frac{S_1(R,t_2)}{AR} + \frac{\nu S_o(R,t_2)}{1-\nu} \tag{117c}$$

where,

$$S_1(R,t_2) = \frac{\pi}{A} \sum_{i=1}^{\infty} \alpha_i^o J_1(\Omega_i R) e^{-(\Omega_i/2A)^2} \cos 2\pi R_i t_2 \tag{117d}$$

$$S_o(R,t_2) = \frac{\pi}{A^2} \sum_{i=1}^{\infty} \alpha_i^o \Omega_i J_o(\Omega_i R) e^{-(\Omega_i/2A)^2} \cos 2\pi R_i t_2 \tag{117e}$$

and

$$\alpha_i^o = [\frac{\pi}{2} \Omega_i J_o^2(\Omega_i)]^{-1} \tag{117f}$$

The dimensionless displacement

$$\bar{u}(.07, t_2) = U_s(.07)-S_1(.07, t_2)$$

is shown in Fig. (8). The wave nature of the solution is clearly evident in this graph. The waves originating at the heated spot propagate out to

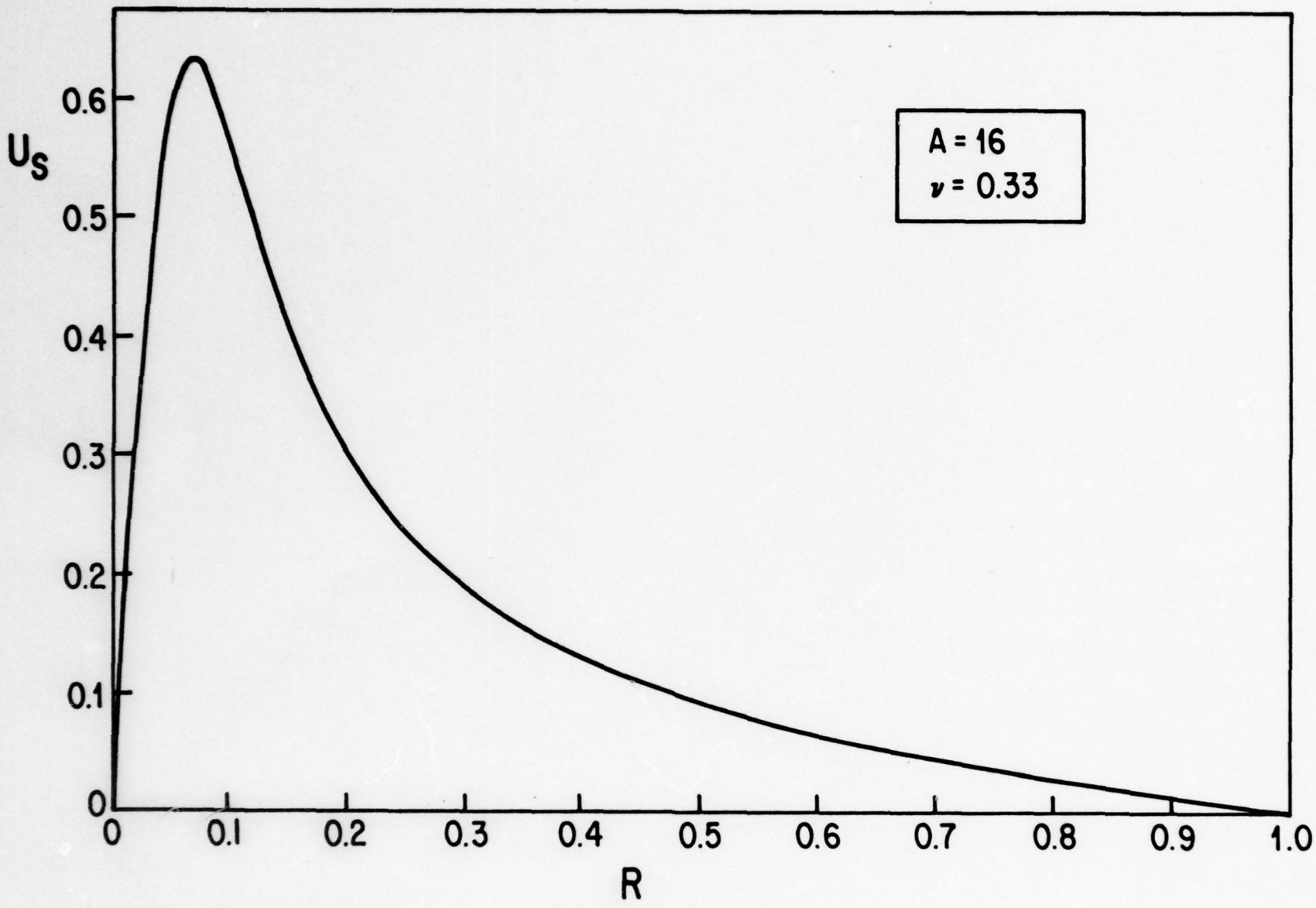

Figure 7: In Plane Quasi-Static Displacement $U_S(R)$ vs. R

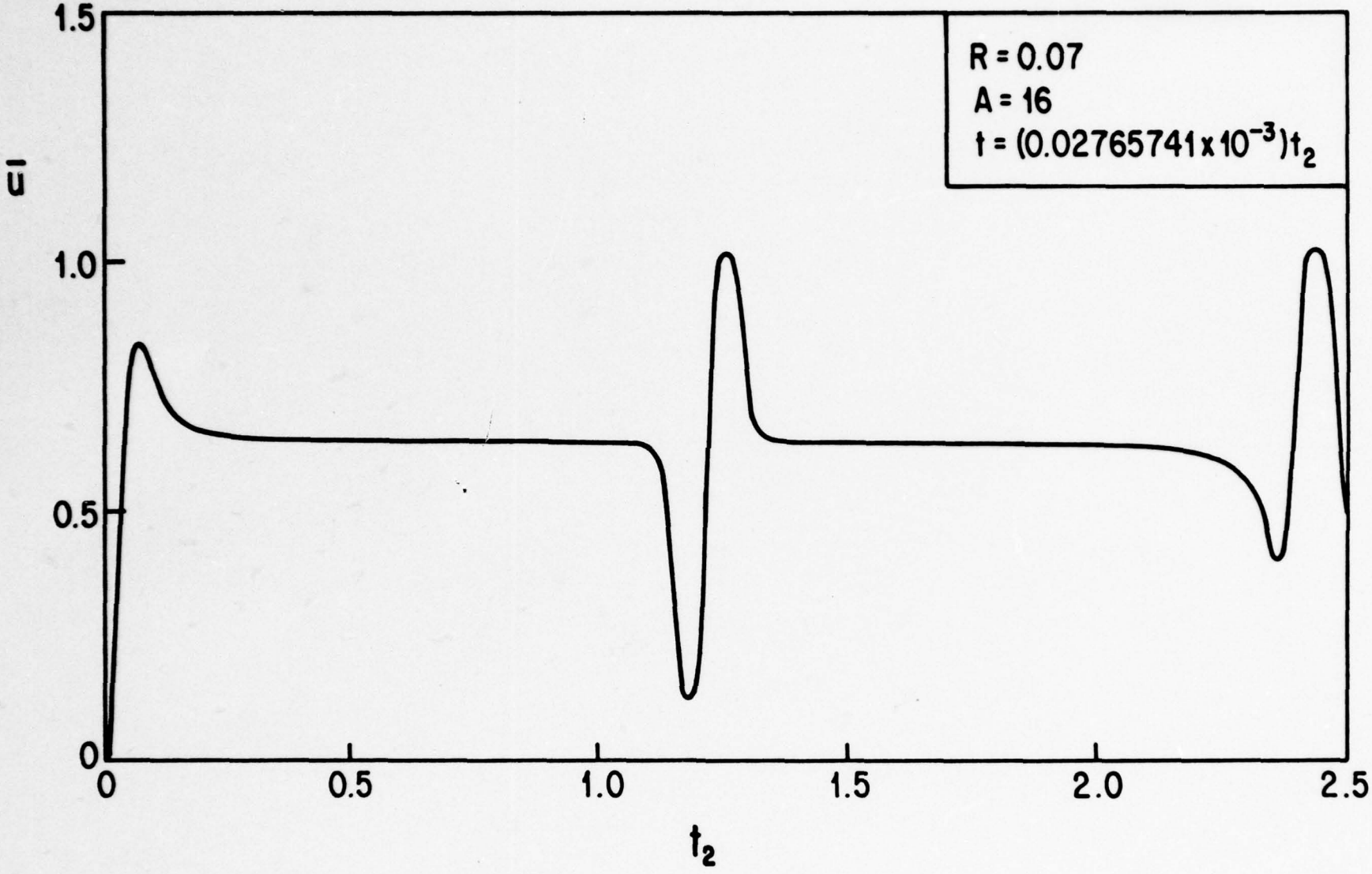

Figure 8: In Plane Displacement $\bar{u}(R, t_2)$ vs. t_2

the clamped boundary are reflected and then propagate back again towards the center of the plate. The passage of these waves at R=.07 is clearly seen in this graph. Since the maximum normal forces occur at the center of the plate, we plot

$$\bar{N}_{rr}(0,t_2) = \frac{N_{rr}(o,t_2)}{N_o} = \frac{N_{\theta\theta}(o,t_2)}{N_o} \tag{118}$$

in Fig. (9). In view of (117),

$$\bar{N}_{rr}(0,t_2) = -\frac{1}{2}[N_{RS}(0) + \frac{1+\nu}{2(1-\nu)} S_o(0,t_2)]$$

$$= \bar{N}_{\theta\theta}(0,t_2) \tag{119a}$$

since

$$S_o(0,t_2) = \sum_{i=1}^{\infty} K_i \cos 2\pi R_i t_2 \tag{119b}$$

$$= \lim_{R\to 0} \frac{2S_1(R,t_2)}{AR} \tag{119c}$$

with

$$K_i = \frac{\pi}{A^2} \alpha_i^o \Omega_i e^{-(\Omega_i/2A)^2} \tag{119d}$$

An examination of K_i reveals that 30 terms are sufficient to obtain $S_o(0,t_2)$ to three significant figures accuracy. The dimensionless normal force $\bar{N}_{rr}(0,t_2)$ is shown in Fig. (9).

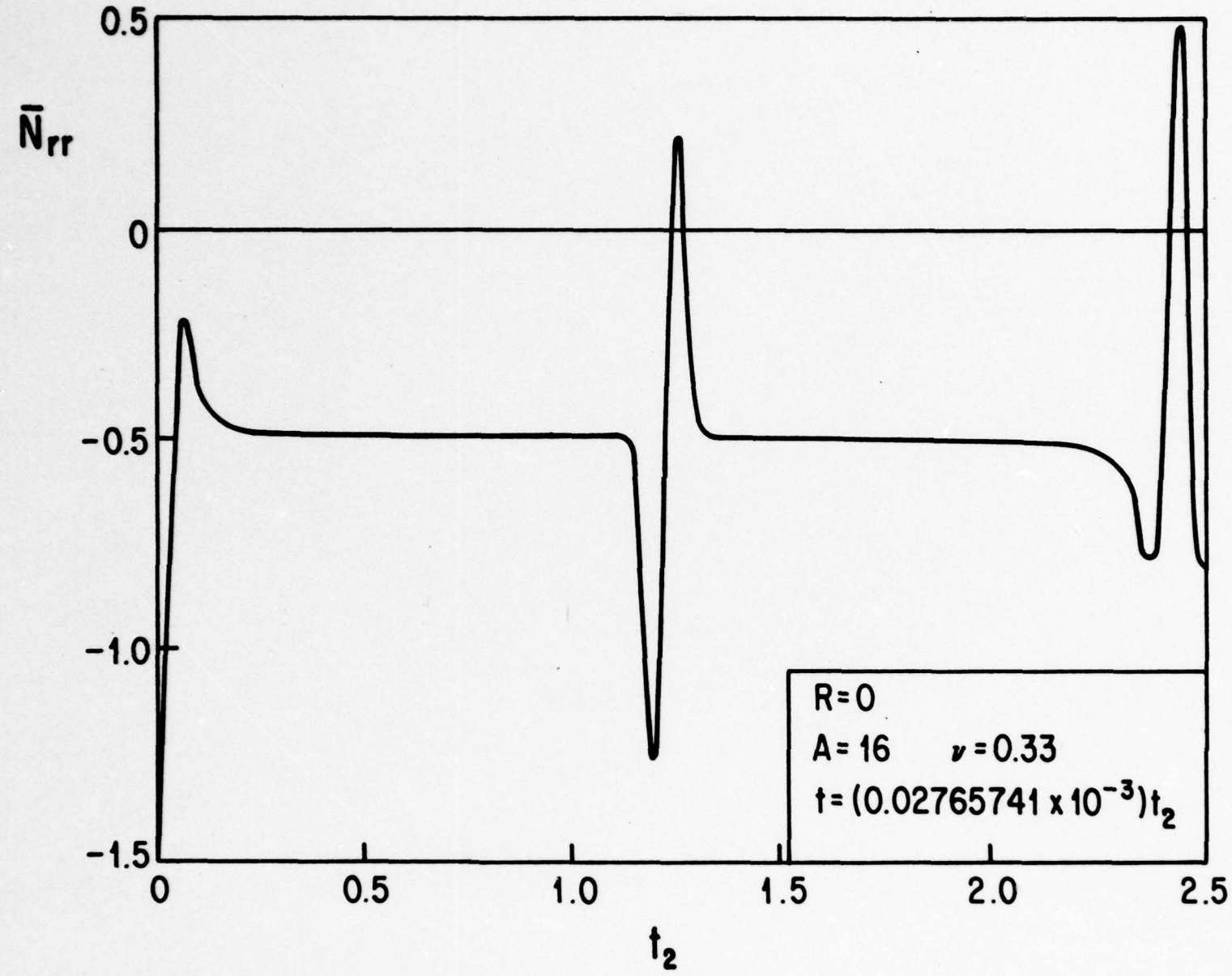

Figure 9: In Plane Forces : $\bar{N}_{rr}(R, t_2)$ vs. t_2

7.0 EXPERIMENTS.

The measurements performed during the initial phase of the study of Laser interaction with finite structures have been based on the concept that the object of the investigation is to provide a careful comparison between experimental data concerning Laser generated thermoelastic deformations and stresses in finite structures with the theory of such processes.

It is clear that a considerable quantity of variable quality experimental evidence has indicated that the mechanical impulse transferred to a target by a Laser pulse could, in general, be understood in terms of material evaporation and removal, and surface plasma generation with and without subsequent plasma heating, possibly involving the creation of LSC & LSD waves in the plasma. Most of these studies have involved the use of either piezoelectric detectors or ballistic impulse detection of gross target motion, both in vacuum and in air. However, at least in the unclassified literature, relatively little effort has been directed toward an understanding of the Laser excitation of elastic oscillations in finite structures. Since these phenomena are of significance in the theoretical treatment of plate dynamics, and since induced stress waves and target oscillations could be of practical value, we felt that a careful comparison of theory and experiment would be both useful and interesting.

It is immediately clear that any study of the dynamic motion of a finite structure could involve the thermoelastic induced motion of the target in addition to any motion induced via a plasma shock or

material blow off. Therefore, our approach to this problem has involved a detailed theoretical and experimental investigation of the purely thermoelastic induced motion of a circular thin plate clamped in such a manner that the plate has zero displacement and slope at its outer free edge. The dimensions of the clamp ring are outer radius 14.6cm, inner radius 11.45cm, thickness 5.7cm, and mass 11.5kg. This clamp ring is mounted in a horizontal plane by means of three support rods which serve to connect the clamp mount to a horizontal plate loaded uniformly with 460kg of lead. This technique is necessary because access to the rear surface of the target plate is required, and the Laser impulse is easily capable of inducing large amplitude oscillations in the clamp ring when mounted in a vertical position.

The target consisted of a type 304 stainless steel circular plate, thickness 19.5 mil (4.95×10^{-2}cm). The density of the target material is 7.788 G cm^{-3}, total mass 260.05 G. This target material was chosen for two reasons; it is reasonably typical of materials used in the aerospace industry, and the thermal diffusivity is sufficiently low (4.1×10^{-2} $cm^2 sec^{-1}$) so that the thermoelastic effect is reasonably large.

The experimental apparatus utilized for this investigation is outlined in Fig. 10. The laser used was a Holobeam model 630-Q Nd;Glass system. This laser produces an output pulse (in the Q switched mode) of approximately 3 joules, with a pulse width of approximately 40×10^{-9}sec. The output beam is about 1cm in diameter, with a beam divergence of 2 m rad, at an output wavelength

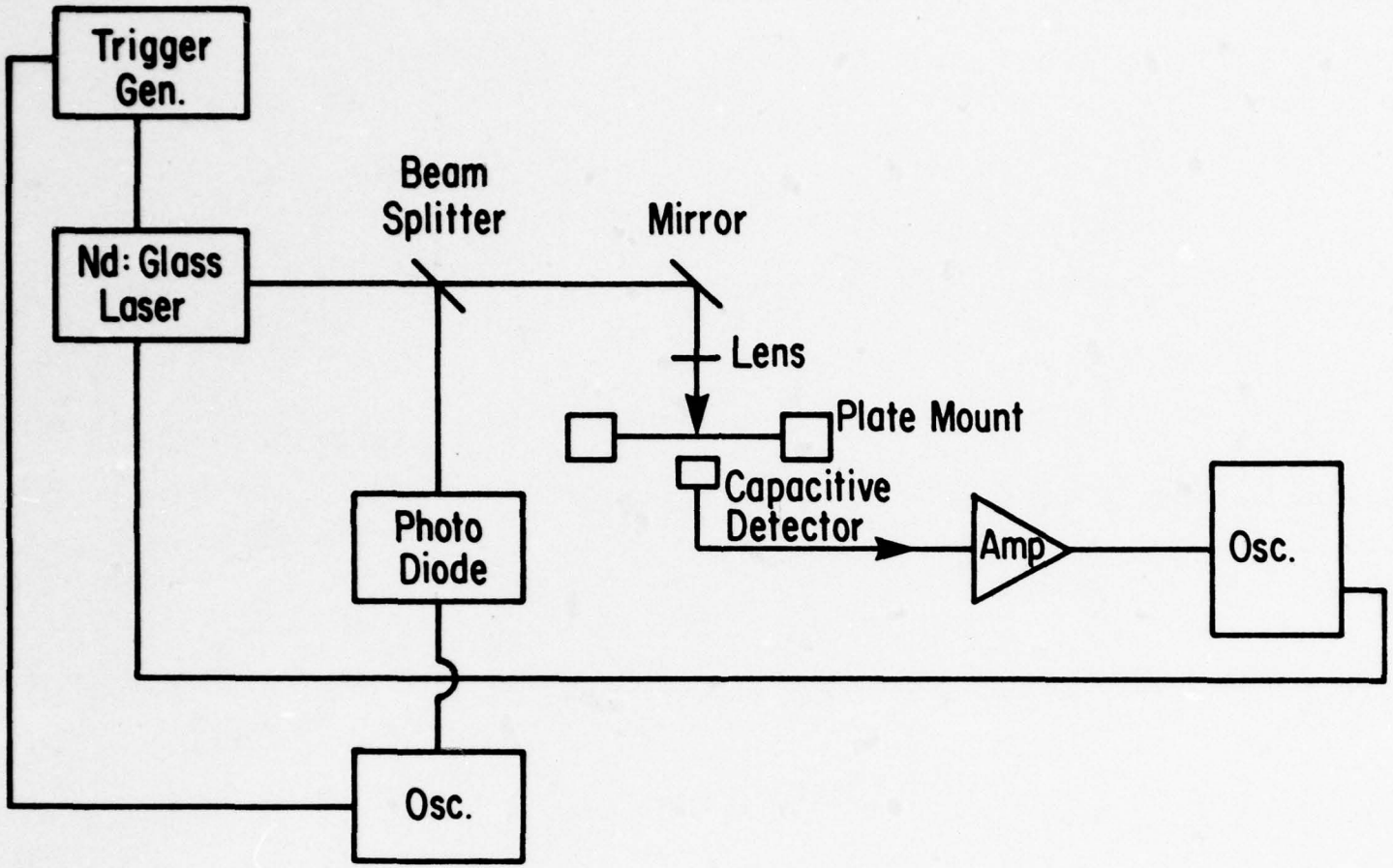

Figure 10: Experimental Apparatus

of 1.06μ. The beam is reflected from a Cu mirror so that it irradiates the target at perpendicular incidence. The direct beam from the laser has an intensity of the order of 100 MW/cm^2, which is more than sufficient to vaporize the target surface, which was not desired in this experiment. Consequently, the beam was expanded using a negative focal length lens to the point below which surface vaporization occurs. In order to insure that the surface irradiation was axially symmetric, the beam was directed after expansion through a circular aperture which defines the area of the plate irradiated by the laser, and insured that the laser irradiated the target at its center. This was done in order to inhibit the generation of non-axially symmetric mode oscillations in the target.

The beam splitter in the beam served to deflect a small portion of the input beam into a Korad Photodiode detector so that the laser pulse energy and power can be monitored. The laser Q switched pulse can, of course, be varied in energy by varying the capacitor discharge voltage, but this is accompanied by a change in the output pulse width. Consequently, the experiments were performed at a constant discharge voltage corresponding to an output energy of approximately 2j. Under these conditions the beam power density was held to a point such that no surface plasma was generated nor melting induced, but such that the surface temperature, based upon Bechtel's treatment [3], was calculated to be close to the melting point.

It was considered desirable to investigate the plate dynamic response resulting from the thermoelastic stress utilizing a method which did not require physical contact with the plate, since such

contacts introduce boundary conditions which may perturb the system dynamic response. Since the absolute amplitudes of the stress waves generated by the laser pulse are difficult to predict, owing to uncertainties in such parameters as the reflection coefficient, specific heat, and thermal conductivity as a function of surface temperature, it was desirable to provide a detection system capable of detecting very small amplitudes of the resulting plate oscillations.

Consequently, the plate motion induced by the laser pulse was initially detected using an optical interferometer. However, since the amplitude of the induced motion was in fact relatively large, a much simpler detection method, as shown in Fig. 10 was used. This consists of a Bruel & Kjaer model MM004 capacitive transducer and associated circuitry. The amplified signal is displayed on a Tektronix 545B oscilloscope and photographed. The detector was mounted at a separation of 1mm from the rear surface (away from the laser), at the center of the plate.

The oscilloscope is triggered from a signal derived from the Q-switch Pockels cell trigger, either in the normal sweep or delayed sweep mode. In this manner, the plate motion is known in time with respect to the occurrance of the laser pulse, and may be examined at any time during the oscillation utilizing the variable time delay of the delaying sweep.

Knowing the detector sensitivity, the plate surface to detector separation, the amplifier gain, the capacitor polarization voltage, and the oscilloscope vertical sensitivity, the overall sensitivity of the detector is known. Therefore, the amplitude of the plate

oscillation can be directly determined from the oscilloscope traces. In our case, the total sensitivity of the detection system is 1.905×10^{-3} volts/in. The maximum amplitude of the Laser induced thermo-elastic oscillations observed in this experiment was 1.3×10^{-3} in, or roughly 6.7% of the plate thickness. Under these conditions, one is confident that the general assumptions of plate theory are valid.

The temperature rise at the rear surface of the target plate was monitored using a thermistor detector. Since, for the values of plate thickness, thermal diffusivity, and pulse width used in this experiment the plate is thermally thin, the temperature at the rear surface is a valid measure of the total energy absorbed. The data then indicate an absorbed energy of 1.16 joule, which is consistent with estimates of the reflection coefficient at 1.06μ and the reflection coefficient of the Cu mirror. This value of absorbed energy then yields an estimate of the surface temperature of 1×10^{3} °C. which is significant only in that it agrees with the non-vaporization or melting assumption. It is not used in our analysis of the data, since we are focusing our interest on the plate oscillation induced by the laser impulse.

The general features of the plate dynamic response are illustrated by the oscilloscope traces shown in Figs. 11-14. These figures are oscilloscope traces for various sweep speeds of the plate oscillations induced by the laser pulse. Several general features of the plate response can be immediately seen in these traces. First, the initial response of the plate consists of a rapid motion in a direction toward the face of the plate irradiated by the laser.

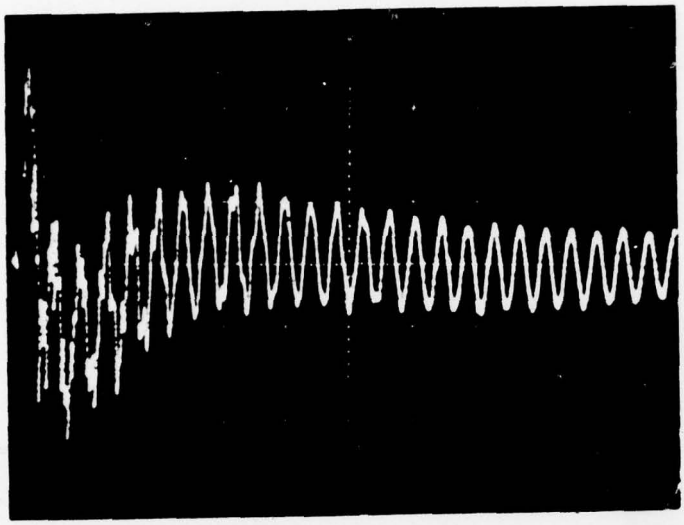

FIGURE 11

Plate Response - Sweep Speed 20 msec/cm. 0.1 v/cm

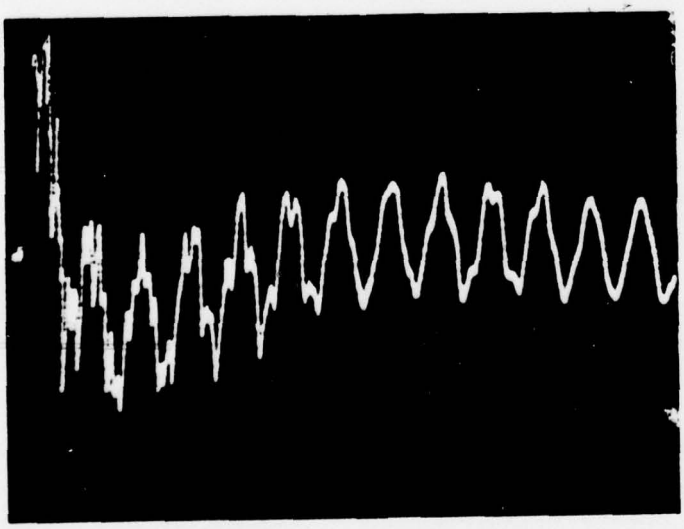

FIGURE 12

Sweep Speed 10 msec/cm.

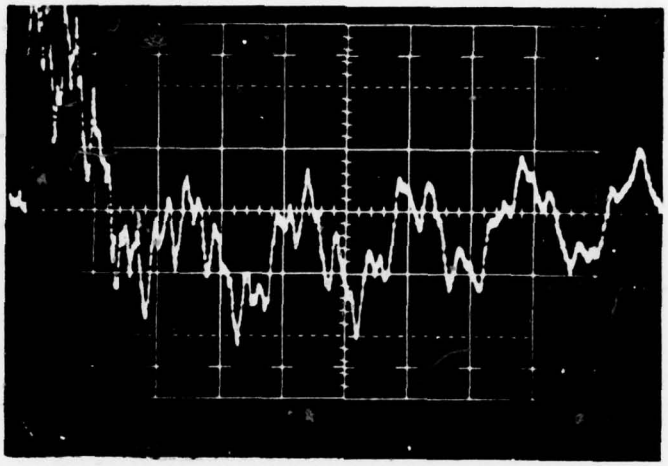

FIGURE 13

Sweep Speed 5 msec/cm

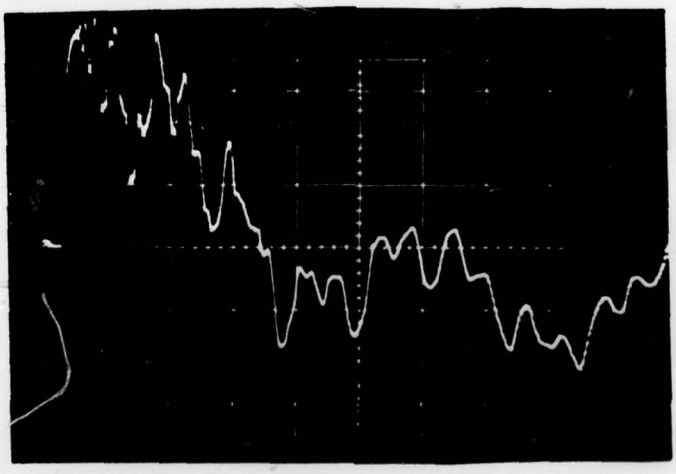

FIGURE 14

Sweep Speed 2 msec/cm

This would be expected if the primary excitation of the plate were by thermoelastic effects. An impulse arising from surface blow off, plasma formation, or thermal effects arising from expansion of the air in contact with the heated surface would be expected to induce initial motion in the opposite direction. Second, the induced plate oscillations contain many higher order modes which have been included in the theoretical model of this process. It is clear that, as expected, these higher order modal frequencies are damped at varying damping rates, so that after a time of the order of 120 m sec, the plate can be seen to be oscillating in its fundamental (i.e., lowest order mode) frequency. As mentioned previously, we have not modeled these variable damping rates in the theoretical treatment of this problem. We have made use of the fact that the plate ultimately oscillates in its lowest order mode to obtain the necessary material constants for use in the theoretical model, as discussed in Appendix II.

Third, the general response of the plate consists of the initial transient, the fundamental and higher order mode oscillations, and, in addition, a superimposed exponential relaxation response, associated with an effective time constant of the order of 17 m sec. That this portion of the plate dynamic response is associated with laser heating is shown by the fact that it is absent when the plate oscillations are induced by mechanical impulse. This is discussed in Appendix II. It is attractive to associate this effect with a possible thermal pre-stress condition, and experiments relating to that effect are continuing. To date, however, we have not included a model of this effect in our theoretical treatment.

The comparison, then, between the theoretical calculations of the plate dynamic response and the experimental results is performed in the following manner. The theoretical response curve (Fig. 5) is based upon material constants chosen so as to agree with the actual observed fundamental mode frequency, as discussed in the Appendix II. On this curve, the point on the time scale (1.0) then corresponds to a time of 8.33 m sec., and the other time points are correspondingly known. The theoretical curve (Fig. 5) is then mounted on a flat surface, and a transparency made from the oscilloscope trace is projected onto the theoretical curve. The magnification of the optical system is then varied so that the time scale of the oscilloscope trace agrees with the horizontal (time) scale of the theoretical curve. Then, maintaining the time scale fixed, the flat surface on which the theoretical curve is plotted is simply rotated so that the vertical (amplitude) scales are normalized at any arbitrary point. The projection of the experimental curve is then simply plotted directly onto the theoretical curve, yielding the comparison between theory and experiment shown in Fig. 15. This figure indicates the comparison in response over a time corresponding to two fundamental periods, or about 17 m sec. Comparison of the theoretical curve and the experimental data taken at a delay time of 7 m sec, using the variable delay of the triggered sweep, is shown in Fig. 16.

Since, as discussed previously, we have not included a consideration of the variable higher order mode damping in our model, it is not particularly useful to extend our comparisons much beyond a time scale of 20 m sec. In fact, it is clear from the comparison of Fig. 15 that

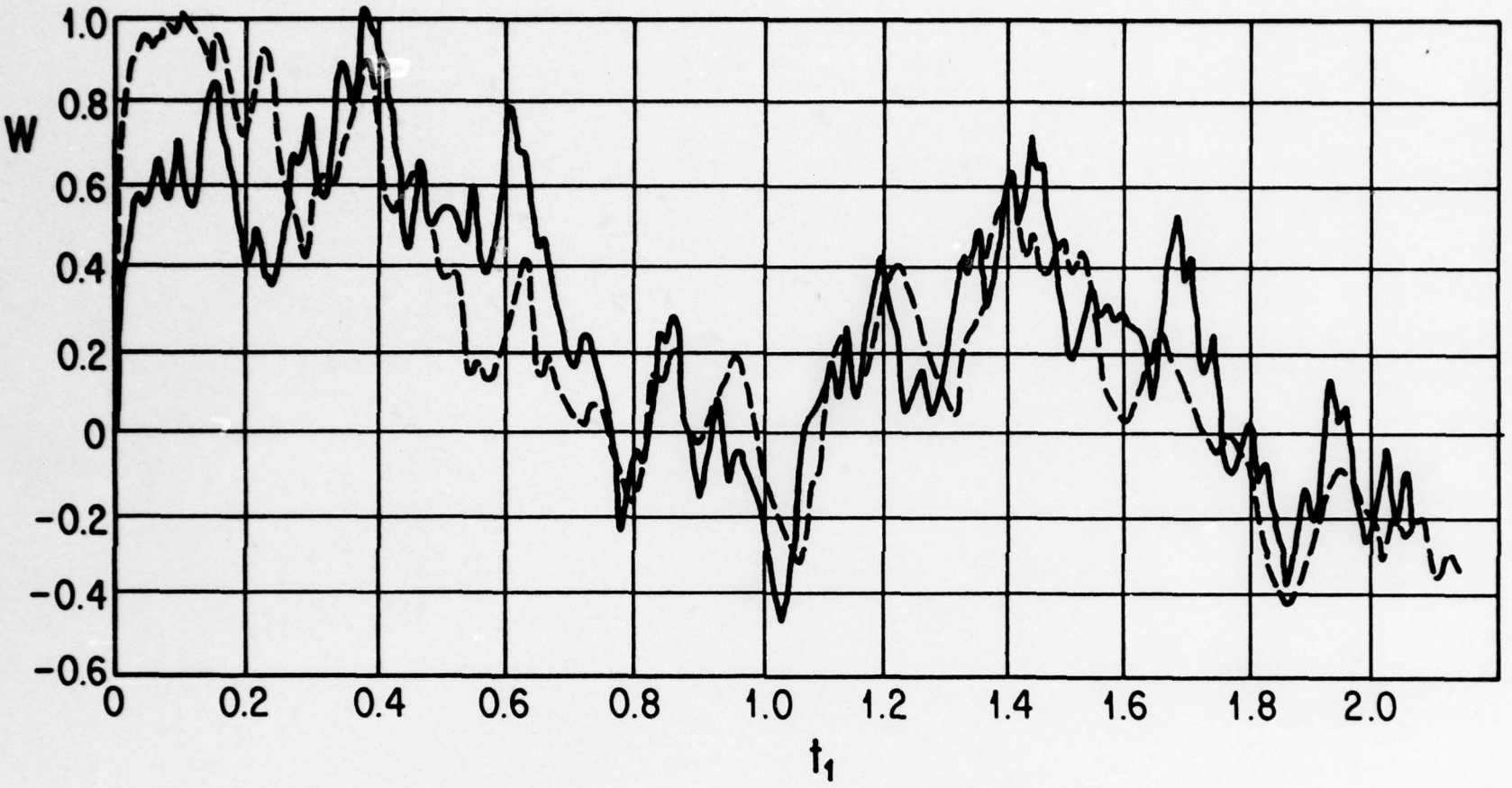

Figure 15: Comparison of Theory and Experimental Data

Horizontal Scale – Units of $T=1/f_0$, f_0 = fundamental frequency (120 Hz)
Vertical Scale – Experimental Data expanded by x 2.
Theoretical Scale Arbitrary
Theoretical Data ——
Experimental Data – – – –

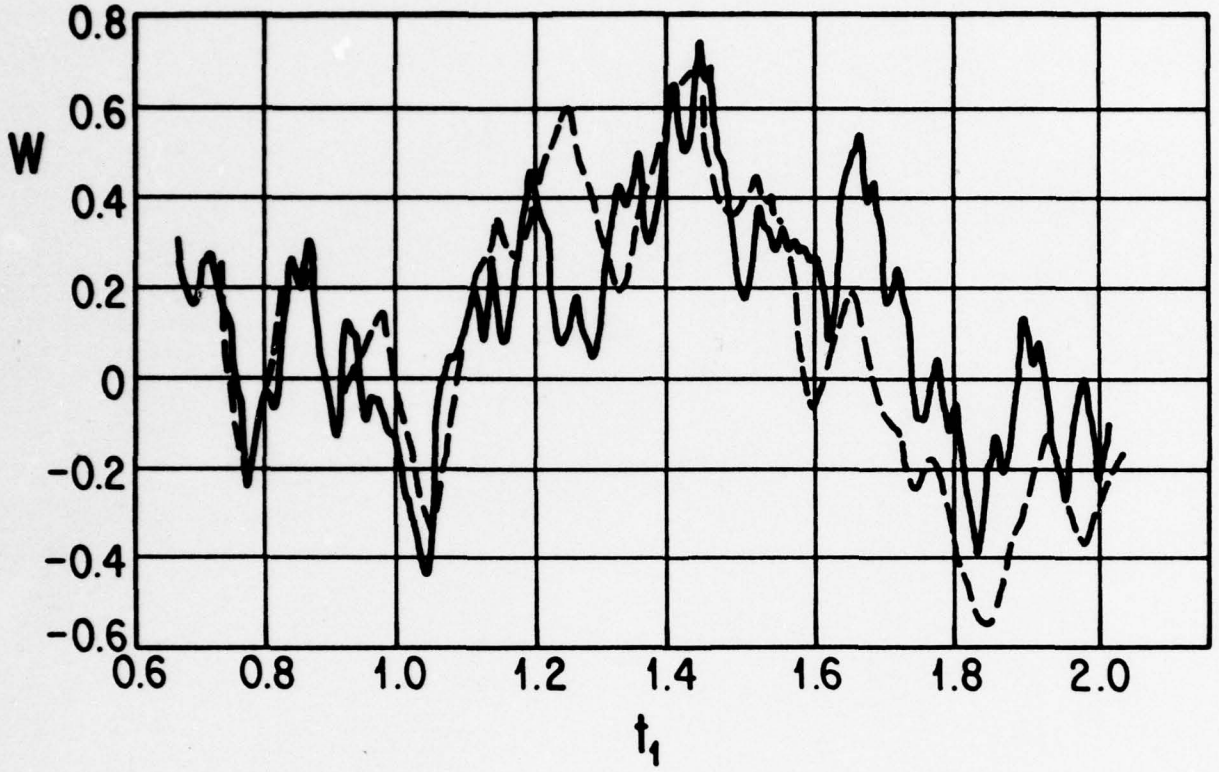

Figure 16: Comparison of Experimental Data vs. Theoretical Model - Delay 7 msec.

Horizontal Scale - Units of Fundamental Period $T = 1/f_1$

several of the higher order mode frequencies have already sufficiently decayed and they are not contributing significantly to the actual plate response.

Using the comparisons illustrated in Fig. 15 and 16, it seems clear that the general features of the response are predicted quite reliably. We believe that the experimental data can be taken as a verification of the thermoelastic model of the laser interaction at this power level.

8.0 CONCLUSIONS

(a) A mathematical model of the Laser induced thermoelastic motion of a plate was derived. The model consists of three partial differential equations with associated boundary conditions. Two of these equations decouple and characterize plate flexure. The remaining equation describes plate stretching.

(b) Laser induced heating is incorporated into the model by using Bechtel's surface heat generation model [3].

(c) The equations were used to solve the problem of a thin circular plate clamped at its boundary. The circular plate is subjected to Laser irradiation at its center, and normal to the plate surface.

(d) Laboratory experiments were performed to measure the center deflection of the plate under Laser irradiation. The results of these experiments compare well with those obtained by calculations using the mathematical model.

REFERENCES

1. Reismann, H., Pawlik, P.S., Elastokinetics - An Introduction to the Dynamics of Elastic Systems, West Publishing Co., St. Paul, 1974.

2. Boley, B.A., Weiner, J.H., Theory of Thermal Stresses, John Wiley and Sons, New York, 1960.

3. Bechtel, J.H., "Heating of Solid Targets With Laser Pulses", J. Appl. Phys., V. 46, no. 4, April 1975, pp. 1585-1593.

4. Watson, G.N., A Treatise on the Theory of Bessel Functions, 2nd. ed., Cambridge Press, London, 1966.

5. Ready, J.F., Effects of High-Power Laser Radiation, Academic Press, New York, 1971.

APPENDIX I: NUMERICAL EVALUATION OF $g_i(t)$

In order to resolve the forced transverse motion problem in section 6.1 it is necessary to evaluate the function

$$g_i(t_1) = M(t_1) - 2\pi R_i \int_0^{t_1} M(\theta) \sin 2\pi R_i (t_1 - \theta) d\theta \qquad \text{(A-1)}$$

where $M(t_1)$ is defined by (93). To simplify the forthcoming analysis we will omit the subscript i on g_i, 1 on t_1 and let $\omega = 2\pi R_i$. Then (A-1) can be rewritten as follows:

$$g(t) = M(t) - F(t) \sin \omega t + G(t) \cos \omega t \qquad \text{(A-2)}$$

where

$$F(t) = \omega \int_0^t M(\theta) \cos \omega\theta d\theta \qquad \text{(A-3)}$$

$$G(t) = \omega \int_0^t M(\theta) \sin \omega\theta d\theta \qquad \text{(A-4)}$$

We wish to evaluate g(t) at a discrete set of points in the interval $0 \le t \le t_{max}$. First, divide the interval into 2N subintervals of length

$$\Delta t = \frac{t_{max}}{2N} . \qquad \text{(A-5)}$$

Let $t_j = j\Delta t$ for $j = 0,1,2,\ldots,2N$. (A-6)

We note from (A-3) and (A-4) that the values of F and G at the instants of time t_{2k}, $k = 1,\ldots,N$ can be evaluated consecutively as follows:

$$F_k \equiv F(t_{2k}) = \omega \int_0^{t_{2(k-1)}} M(\theta) \cos \omega\theta d\theta + \omega \int_{t_{2(k-1)}}^{t_{2k}} M(\theta) \cos \omega\theta d\theta$$

or, in other words,

$$F_k = F_{k-1} + \Delta F_{k-1} \qquad \text{(A-7)}$$

$$G_k = G_{k-1} + \Delta G_{k-1} \qquad k = 1,2,\ldots,N \qquad \text{(A-8)}$$

where,

$$\Delta F_{k-1} = \omega \int_{t_{2(k-1)}}^{t_{2k}} M(\theta)\cos \omega\theta d\theta \qquad \text{(A-9)}$$

$$\Delta G_{k-1} = \omega \int_{t_{2(k-1)}}^{t_{2k}} M(\theta)\sin \omega\theta d\theta \qquad \text{(A-10)}$$

and $F_o = G_o \equiv 0$.

To evaluate the integrals (A-9) and (A-10), we use a second order Lagrange interpolation formula to approximate $M(\theta)$ on the interval $(t_{2(k-1)}, t_{2k})$, i.e.,

$$M(\theta) \cong Y_{2k-2}L_{2k-2} + Y_{2k-1}L_{2k-1} + Y_{2k}L_{2k} \qquad \text{(A-11)}$$

where

$$\left.\begin{aligned} L_{2k-2} &= (\theta-t_{2k-1})(\theta-t_{2k})/(2(\Delta t)^2) \\ L_{2k-1} &= (\theta-t_{2k-2})(t_{2k}-\theta)/(\Delta t)^2 \\ L_{2k} &= (\theta-t_{2k-2})(\theta-t_{2k-1})/(2(\Delta t)^2) \end{aligned}\right\} \qquad \text{(A-12)}$$

where, $Y_j = M(t_j)$ $\quad j=0,1,\ldots,2N.$

Substitution of (A-11) and (A-12) into (A-9) and (A-10) yields the results

$$\Delta F_{k-1} = Y_{2k}S_{2k} - Y_{2k-2}S_{2k-2} + \frac{1}{2\Omega}(a_k C_{2k} + b_k C_{2k-2}) + \frac{C_k}{\Omega^2}(S_{2k-2} - S_{2k}) \qquad \text{(A-13)}$$

$$\Delta G_{k-1} = Y_{2k-2}C_{2k-2} - Y_{2k}C_{2k} + \frac{1}{2\Omega}(a_k S_{2k} + b_k S_{2k-2}) + \frac{C_k}{\Omega^2}(C_{2k} - C_{2k-2}) \qquad \text{(A-14)}$$

where,

$$\left.\begin{aligned} \Omega &= \omega\Delta t \\ a_k &= 3Y_{2k}-4Y_{2k-1}+Y_{2k-2} \\ b_k &= Y_{2k}-4Y_{2k-1}+3Y_{2k-2} \\ c_k &= Y_{2k}-2Y_{2k-1}+Y_{2k-2} \\ S_{2k} &= \sin \omega t_{2k} = \sin 2k\Omega \\ C_{2k} &= \cos \omega t_{2k} = \cos 2k\Omega \end{aligned}\right\} \qquad \text{(A-15)}$$

Consequently,

$$g(t_{2k}) = Y_{2k}-F_k S_{2k}+G_k C_{2k}\ , \quad k=1,2,3,\ldots,N. \qquad \text{(A-16)}$$

To check the accuracy of this approximation, the following example, having a closed form solution, was tested.

$$M(t) = e^{-\alpha t} \qquad \text{(A-17)}$$

In this case

$$g(t) = \frac{\alpha^2 e^{-\alpha t} - \omega(\alpha \sin \omega t - \omega \cos \omega t)}{\alpha^2 + \omega^2} \qquad \text{(A-18)}$$

Table (A-1) shows the comparison of the exact result from (A-18) with the approximation (A-16) for the case $t_{max}=1$, N=10, $\omega=2\pi$, $\alpha=1.84$. The agreement with N=10 is seen to be quite good. Further tests with values of ω up to 200π and N=10 indicate that the accuracy does not decrease significantly as ω increases. Another test with $t_{max}=1$, $\omega=2\pi R_{30}$, where $R_{30}=\omega_{30}/\omega_1$, and N=100 was run and the agreement between the exact and approximate values was at least seven and sometimes eight decimal places.

TABLE (A-1)

Test of Numerical Evaluation of g(t)

k	t_{2k}	Exact g(t)	Approximate g(t)
1	.1	.652293	.652290
2	.2	.082762	.082757
3	.3	-.495644	-.495648
4	.4	-.865816	-.865817
5	.5	-.889538	-.889537
6	.6	-.560396	-.560392
7	.7	-.006310	-.006304
8	.8	.559248	.559253
9	.9	.918730	.918732
10	1.0	.933559	.933559

Based on these observations, the final calculations in section (6.1) were run using $t_{max}=2$ and N=200.

APPENDIX II: EXPERIMENTAL DETERMINATION OF PLATE STIFFNESS.

It became clear even during the initial stages of this experiment, in which interferometric techniques were utilized to study the plate dynamic motion, that the fundamental frequencies observed were in general significantly different from those predicted by handbook values of the material constants for our selected target material.

It was therefore considered necessary to perform some calibration experiments relating to the determination of the effective plate stiffness, which determine the predicted plate response to the laser pulse. Several related experimental techniques were used in this regard, namely excitation of the plate oscillations by mechanical impulse, electromagnetic excitation of plate oscillations, holographic analysis of static deflection, and direct measurement of the purely fundamental mode frequencies during the laser excitation.

Since this latter method is most directly related to the main experimental approach, we will describe it first. The circuit outlined in Fig. A1 is used. The signal from the photodiode detector triggers the delaying sweep of the 545B. After a time determined by the variable delay, the main sweep of the 545B is triggered, and the main sweep signal serves as an enable gate to the IC gate circuit. When this gate signal is present, the detected signal from the capacitive transducer is passed to the 5245 electronic counter operated in the period mode. Each time the laser is fired, a measurement is obtained of the fundamental plate frequency by delaying the main sweep trigger until the higher order modes have damped out. The period observed in this manner was then

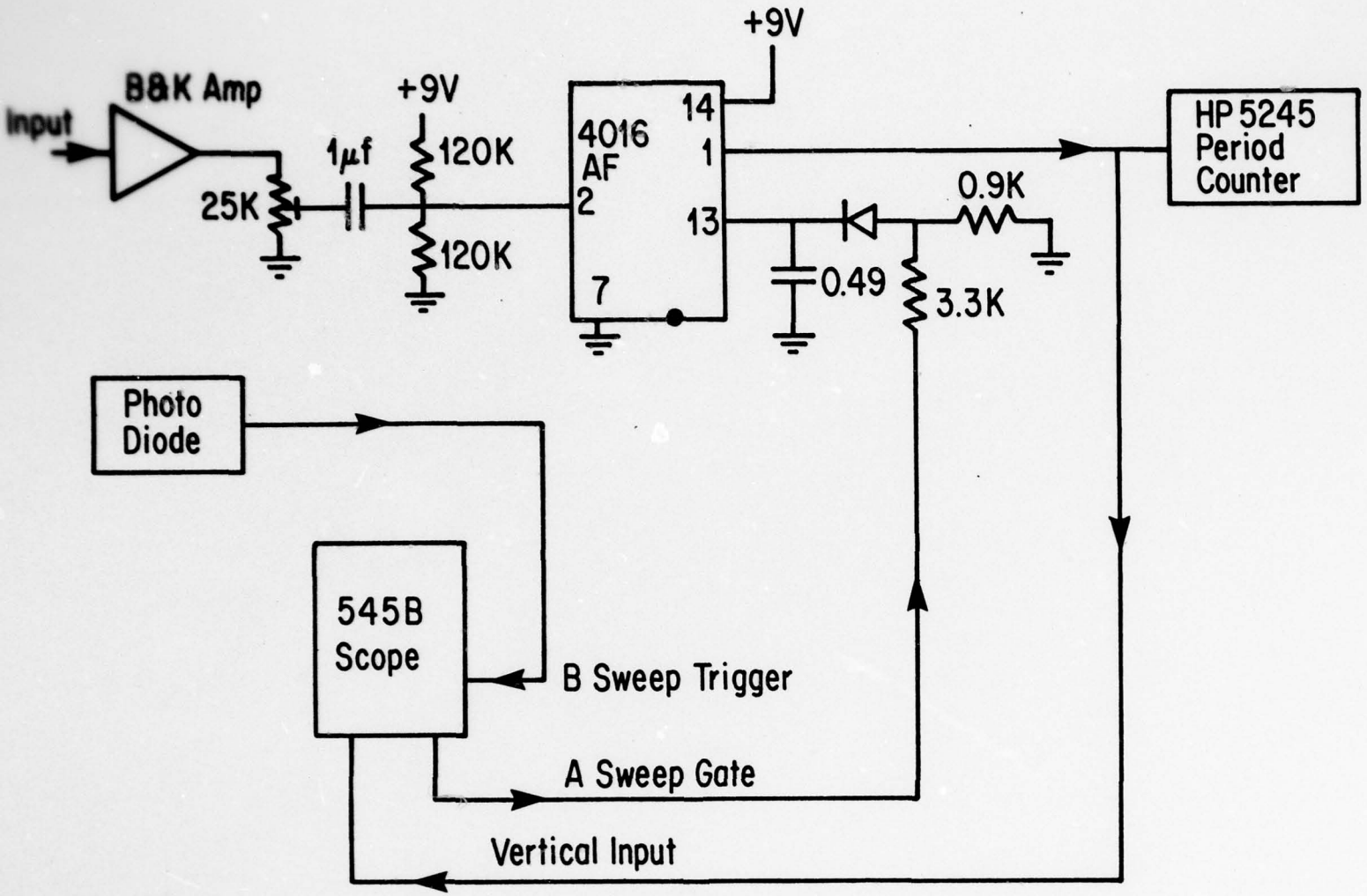

Figure A1: Delayed Gate Detection of Lowest Mode Frequency

a model of this effect in our theoretical treatment.

$(8.2630 \pm 0.0277) \times 10^{-3}$ sec., corresponding to a fundamental frequency of (121.02 ± 0.58) Hz.

The response of the plate to a mechanical impulse was investigated using the apparatus outlined in Fig. A2. In this experiment, the mechanical impulse was produced by allowing a small copper sphere to strike the plate at its center. Since the target plate is mounted in a horizontal position, as discussed in section 7.0 of this report, the sphere is suspended by elastic supports so that it does not contact the plate in its equilibrium position. A signal derived from the interruption of a He-Ne laser beam passing parallel to the plate face was used to trigger the delaying sweep of the oscilloscope in the same manner as the apparatus used in the main experiment. Oscillograms of the plate response to this excitation are illustrated in Figs. A-3 through A-5.

Several conclusions can be reached from these responses. First, it is clear that the initial plate response is in a direction away from the mechanical impulse, as would be expected. This is in fact the opposite effect from the thermoelastic response to the laser impulse. Second, the oscillations induced by the mechanical impulse are symmetric about the baseline. This is in contrast to the laser induced plate response which exhibits an exponential transient in addition to the plate oscillation. We therefore believe that this transient effect is a result of the thermoelastic excitation, and is not characteristic of the plate itself. In addition, the frequency spectrum of the response to this method of excitation contains fewer higher order modes than is the case for thermoelastic excitation.

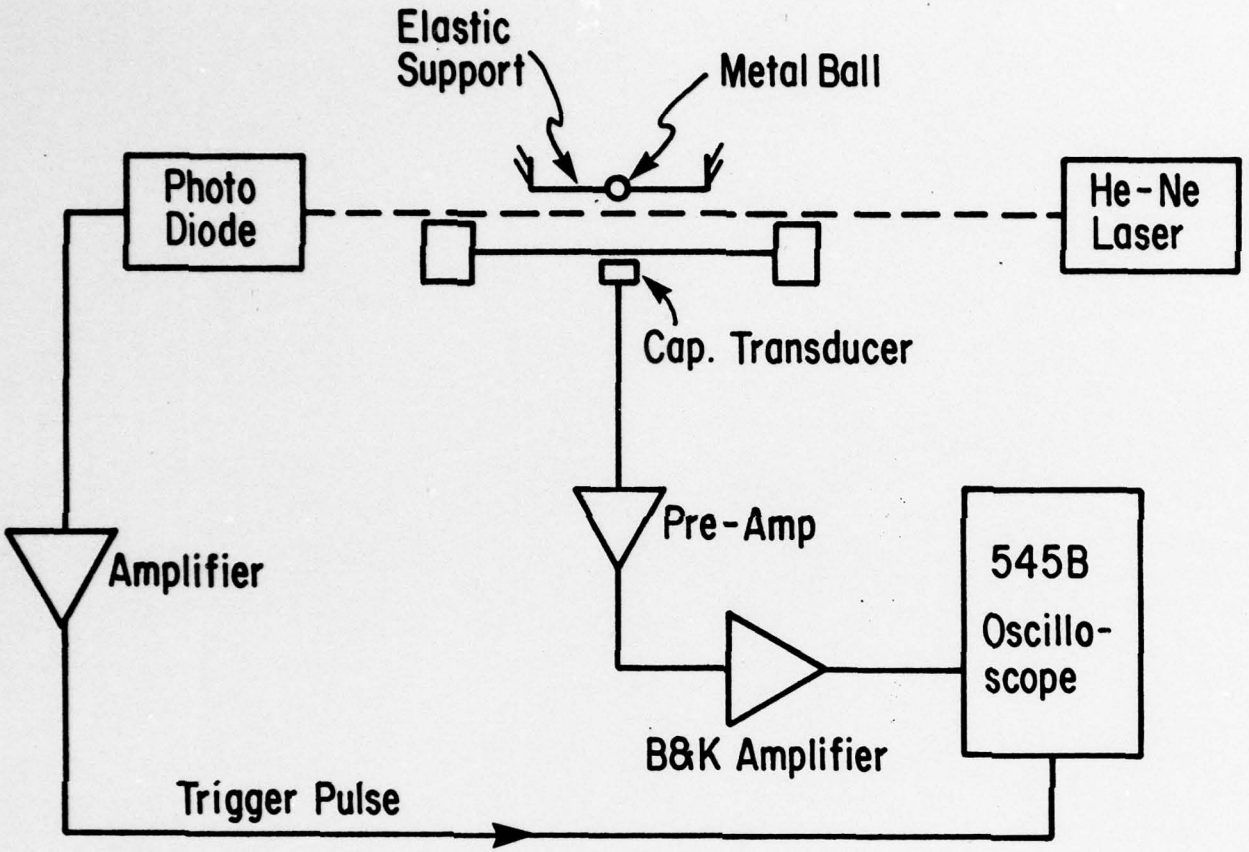

Figure A2: Mechanical Impulse Excitation

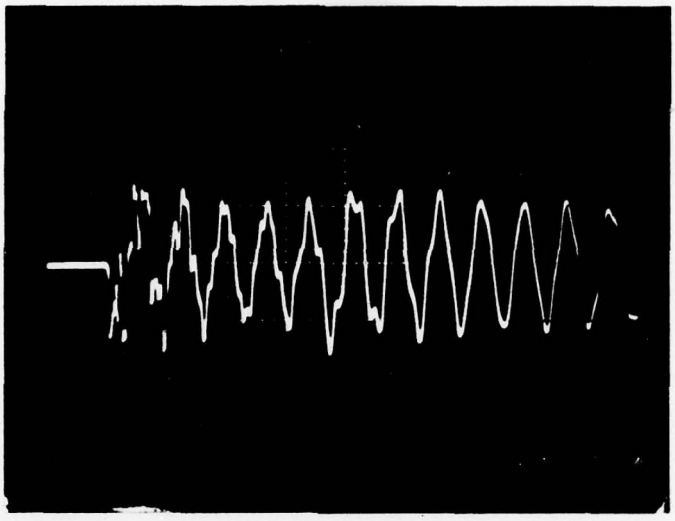

FIGURE A-3

Plate Response to Mechanical Impulse
10 ms/div 5v/div

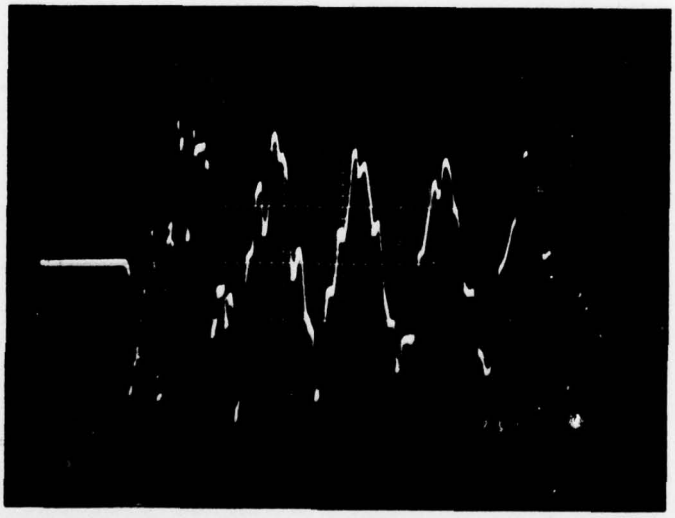

FIGURE A-4

5 ms/div 5v/div

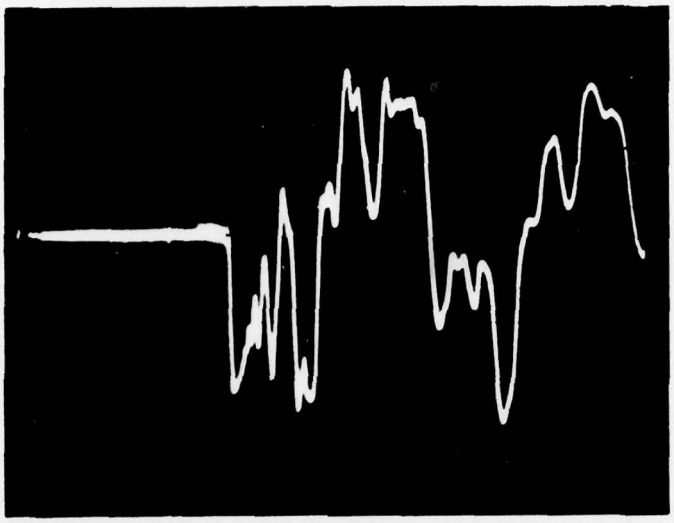

FIGURE A-5

2 ms/div 5v/div

It is clear that they are damped at variable rates, as observed in the laser excitation. Lastly, it can be seen that the fundamental frequency is in agreement with the laser excited frequency, as one would expect.

In order to study the plate vibration frequency spectrum, the apparatus outlined in Fig. A6 has been used. In this experiment, the plate oscillations are excited by means of an electromagnetic transducer (B&K Model 0002) driven by a variable frequency oscillator. The voltage derived from a 390 Ω resistor in series with the transducer is used in the feedback mode to maintain a constant amplitude of the plate excitation as the frequency is varied. This is necessary since the transducer presents an inductive reactance load to the oscillator. Using this apparatus, the various modal oscillation frequencies may be separately excited by the oscillator. The first five modes were easily observable in this test. The observed frequencies, at a plate temperature of 76°F were 120.1, 467, 1055, 1858, and 2900 Hz.

The value of Young's modulus for the material, or perhaps more properly, the effective plate stiffness, may be determined from these data using the relation:

$$f_{ij} = \frac{\lambda_{ij}^2 h}{2\pi a^2}\left[\frac{E}{12(1-\nu^2)\zeta}\right]^{1/2} \qquad \text{(A-19)}$$

where

λ_{ij} = modal eigen value

h = plate thickness

a = plate (free) radius

E = Young's Modulus

ζ = plate density

ν = Poisson's ratio

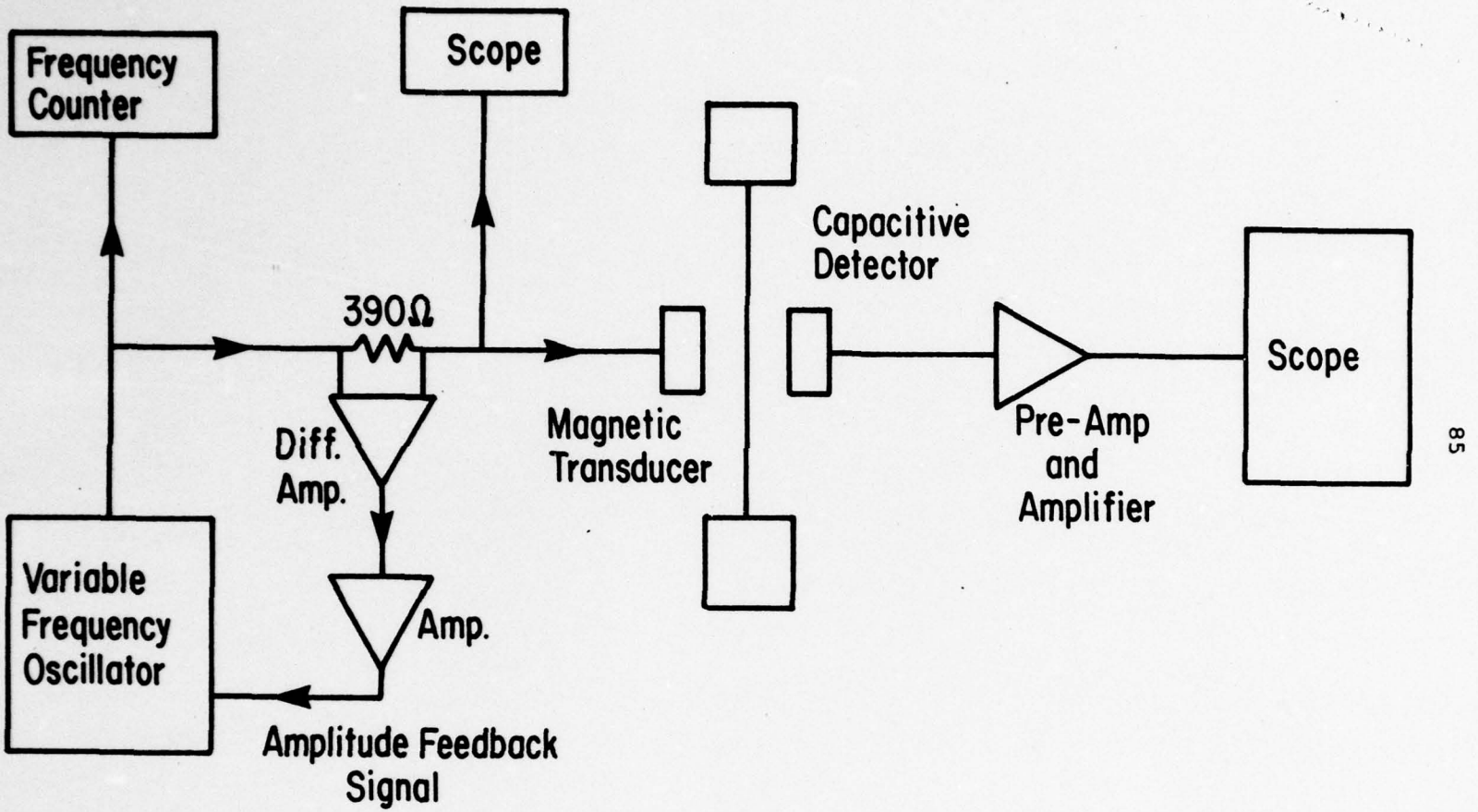

Figure A6: Electromagnetic Excitation of Plate

During the course of this experiment, it became clear that the resonant frequency observed was in fact highly sensitive to the ambient plate temperature. In general, it has been observed that the lowest order mode frequency shifts at a rate of 4.88 Hz/°F. Consequently, the data have been taken at or near the 76°F value mentioned above. We presently feel that this effect is probably due to a thermal pre-stress condition arising from the fact that the thermal masses of the massive clamp and thin plate are greatly different. Therefore, an ambient temperature change affects the plate more rapidly than the clamp. Theoretical analysis of this effect is continuing at present, along with further experimental investigation of the effect of the temperature difference (between clamp and plate) on the resonant frequencies.

In addition, it was considered desirable to investigate the static deflection characteristics of the plate as an independent study of the material constants of the plate. The apparatus used is shown in Fig. A7. Weights of 10, 20, 50, and 100 G were applied to the plate, and double exposure holograms were made of the plate. That is, a hologram of the undeflected plate (no load) was made by exposing the holographic plate, the holographic plate was covered, the load applied, and a second exposure was made. After the hologram was developed and dried, it was replaced in the plate holder and illuminated by the reference beam only. A photograph was then made of the holographic image thus formed. This photograph then shows an image of the plate, superimposed on which is a series of interference fringes resulting from the static deflection of the plate. Displacement

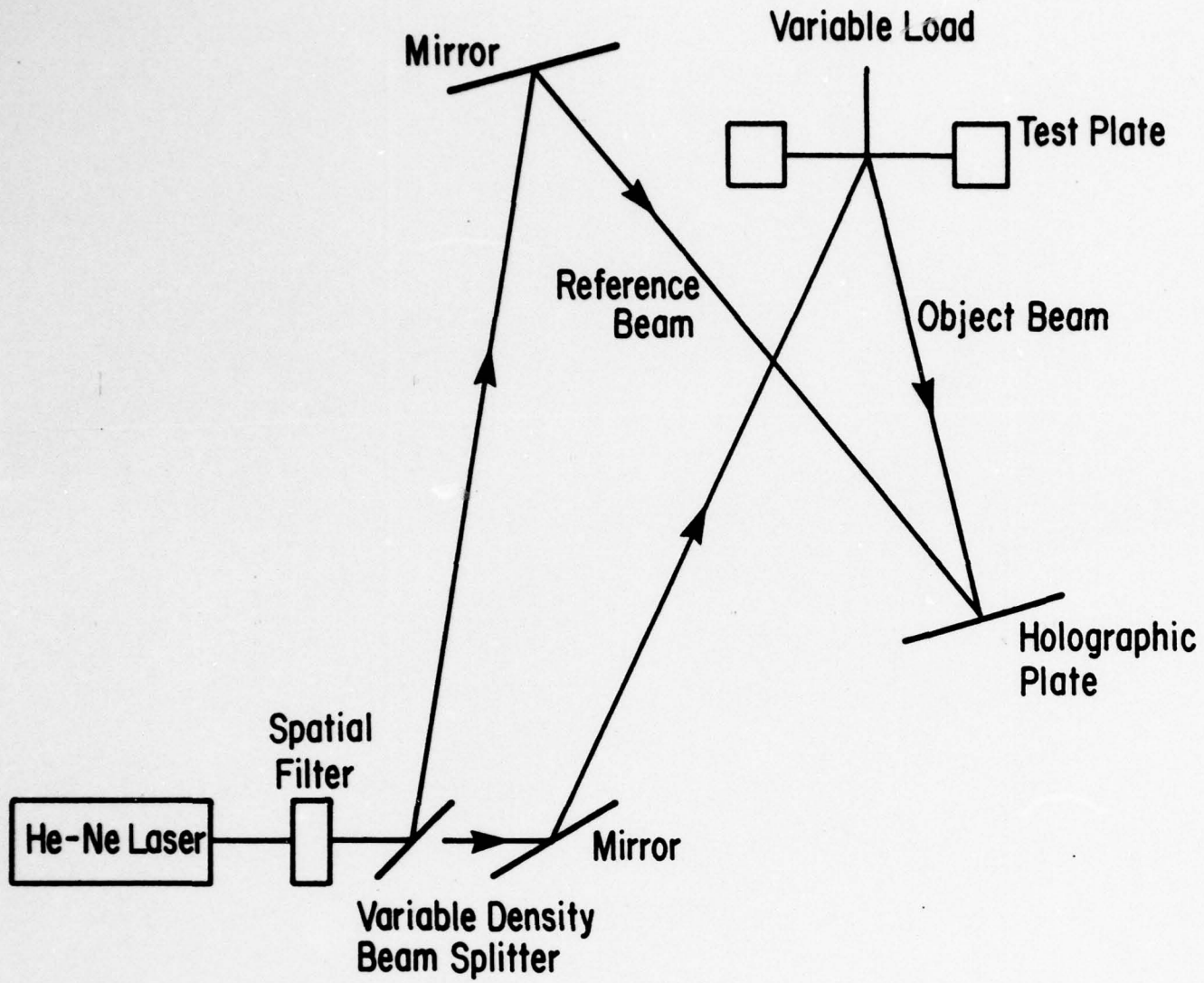

Figure A7: Double Exposure Hologram Test Static Deflection Experiment

values are then determined by counting the interference fringes from the undeflected edge of the plate image to any point on the plate. Since each fringe shift corresponds to a phase shift of $\lambda/2$, where λ is the laser wavelength, and therefore corresponds to a total plate deflection of $\lambda/4$, the displacement can be determined to a precision of $\lambda/4$, approximately, after correction for the incidence and reflection angles. Since the deflections are then determined, the plate characteristics, stiffness and Young's modulus, may be determined in two separate, but related, methods of analysis. First, the equation of the static deflection of a centrally loaded plate is given by:

$$\omega(r) = \frac{P}{8\pi D}\{r^2 \ell n\, r/a + (a^2-r^2)/2\} \tag{A-20}$$

where a=plate radius, r=radial distance from the plate center, P=load, D=plate stiffness. The deflection to be expected at the plate center (r=0) is then:

$$\omega(0) = \frac{a^2 P}{16\pi D} = \frac{3(1-\nu^2)a^2 P}{4\pi h^3 E} \tag{A-21}$$

Therefore, if the observed deflections at the plate center are plotted as a function of the load (Fig. A8), then a least square fit to the data yields a value for the slope from which E may be calculated.

Alternatively, since the deflection, at a given load, is a known function of radial distance, it is clear that the slope of the plate surface, $\frac{dw}{dr}$, will have a maximum value at r=a/e of:

$$\left.\frac{dw}{dr}\right|_{r=a/e} = \frac{3(1-\nu^2)aP}{\pi e h^3 E} \tag{A-22}$$

from which E may also be determined. Note that e=2.7183 ... .

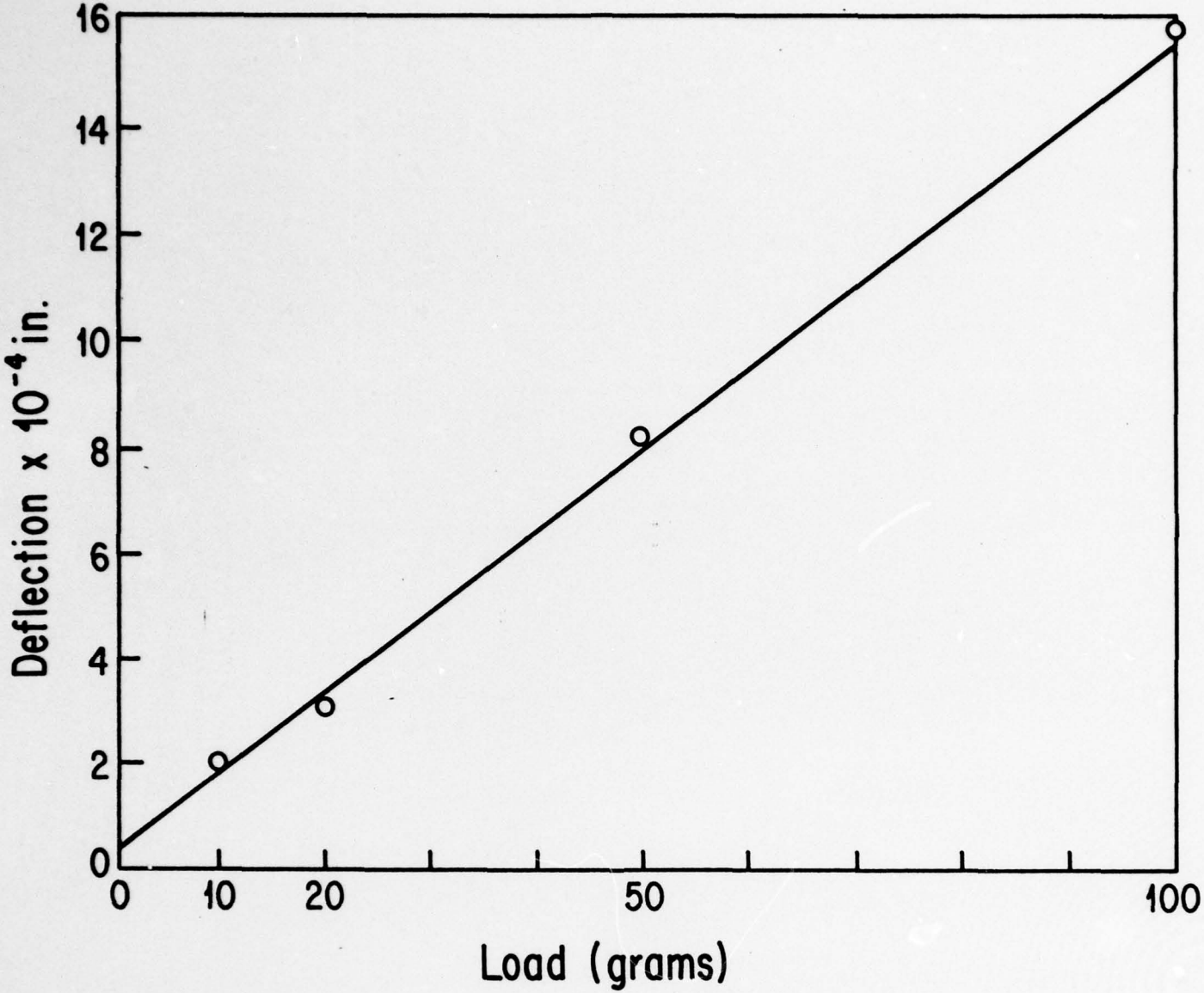

Figure A8: Static Deflection vs. Applied Load

This procedure was carried out for the target plate used in the laser irradiation experiments, and for a non-irradiated sheet cut from the same original sheet.

The results indicated that the values of E determined from equations (A-21) and (A-22) agree to within 1%. However, the value of E determined in this manner for the non-irradiated sample was unreasonably large (of the order of 80×10^6 lb/in^2). Since the values obtained from the two methods of analysis agree, and since the ratio of the experimental value of the slope in equation (A-3) to the experimental value of the slope in equation (A-4), that is:

$$\left.\frac{w(o)}{\frac{dw}{dr}}\right|_{r=a/e} = \frac{ae}{4} \qquad \text{(A-23)}$$

agrees to within 1.5% of the expected value, it is believed that the radial dependence as given in equation (A-23) is correct. It is noted that the experimental deflections in this test were intentionally limited to small values (1.6×10^{-3} in, maximum). It is possible that the large values observed in this test are an additional indication of a thermal pre-stress condition referred to previously.

A more interesting observation, however, was that the value of E determined for the laser irradiated plate was about 1.7 times larger than the non-irradiated plate. During the initial measurements on the laser irradiation results, the plate was of course irradiated many times, and, because the beam was not initially expanded, a laser produced surface plasma was induced several times. Subsequently, the

plate was pulsed repeatedly at lower power density. Consequently, we do not know whether the apparent increase was due to the initial high intensity impulses, the later lower intensity impulses or both. Furthermore, after the second target plate had been used for the thermoelastic study and the required data obtained, we irradiated it at higher power densities, and utilized the electromagnetic transducer (as outlined above) to determine the fundamental resonant frequency. An increase in the value was immediately observed, again raising the question of whether the high power pulse has resulted in an effective increase in plate stiffness. However, until the effects of the thermal pre-stress condition are better understood, we believe it would be premature to assign the observation to a change in the material constants of the plate.